Title:

Does timing matter in radiotherapy of hepatocellular carcinoma?

Authors:

Soha A. Hassan[1,2], Amira A. H. Ali[1], Dennis Sohn[3], Ulrich Flögel[4], Reiner U. Jänicke[3], Horst-Werner Korf[5], Charlotte von Gall[1]

1 Institute of Anatomy II, Medical Faculty, Heinrich-Heine-University, Universitätstrasse 1, 40225 Düsseldorf, Germany.
2 Zoology Department, Faculty of Science, Suez University, Suez 43111, Egypt.
3 Laboratory of Molecular Radiooncology, Clinic and Policlinic for Radiation Therapy and Radiooncology, Medical Faculty of Heinrich-Heine-University, Universitätstrasse 1, 40225 Düsseldorf, Germany.
4 Department of Molecular Cardiology, Heinrich-Heine-University, Universitätstrasse 1, 40225 Düsseldorf, Germany.
5 Institute of Anatomy I, Medical Faculty, Heinrich-Heine-University, Universitätsstr. 1, 40225 Düsseldorf, Germany.

Correspondence: Prof. Horst-Werner Korf, korf@uni-duesseldorf.de

Simple summary

Hepatocellular carcinoma (HCC), which is mostly diagnosed in advanced stage, is highly resistant to antimitotic therapies. Radiotherapy is rarely used in HCC treatment due to the increased risk of radiation-induced liver damage which follows hepatic radiotherapy. To date, it is unknown if this side effect can be reduced if the radiotherapy applied at the proper timing. Our study aims to introduce the concept of chronotherapy to radiobiological cancer research by defining the optimal time point at which the HCC is more radiosensitive, whilst the surrounding HL is more radioresistant to the damaging effects. Our results from *Per2::luc* mice bearing HCCs irradiated at four time points during the day allowed us to define ZT20 (late activity phase) as an optimal time point to apply radiotherapy in nocturnal mice. Translation studies are now required to clarify whether these findings can be confirmed for HCC patients.

Preprints (www.preprints.org) | NOT PEER-REVIEWED | Posted: 29 January 2021 doi:10.20944/preprints202101.0603.v1

Abstract:

This study investigates whether a chronotherapeutic treatment of hepatocellular carcinoma (HCC) may improve treatment efficacy and mitigate side effects on healthy liver (HL). HCC was induced in *Per2::luc* mice which were irradiated at four time points of the day. Proliferation and DNA-double strand breaks were investigated in irradiated and non-irradiated organotypic slice culture (OSC) and *ex vivo* samples by detection of Ki67 and γ-H2AX. OSC proved useful to determine dose-dependent effects on proliferation and DNA damage but appeared unsuited to test the chronotherapeutic approach. Irradiation of *ex vivo* samples was most effective at the proliferation peaks in HCC at ZT02 (early inactivity phase) and ZT20 (late activity phase). Irradiation effects on HL were minimal at ZT20. *Ex vivo* samples revealed disruption in daily variation and down-regulation of all investigated clock genes except *Per1* in non-irradiated HCC as compared with HL. Irradiation affected rhythmic clock gene expression in HL and HCC at all ZTs except at ZT20. Irradiation at ZT20 had no effect on total leukocyte numbers. Our results indicate ZT20 as the optimal time point for irradiation of HCC in mice. Translational studies are now needed to evaluate whether the late activity phase is the optimal time point for irradiation of HCC in man.

Keywords: Clock genes, Hepatocellular carcinoma, Ki67, Radiotherapy, Transgenic *Per2::luc* mice, γ-H2AX.

Introduction

Hepatocellular carcinoma (HCC) occupies the fourth rank of cancer death causes worldwide with a mortality rate of 8.2% (782 000 deaths) and 841 080 new cases in 2018 [1,2]. HCC is characterized by high malignancy as well as fast progression, invasion and metastasis. Moreover, HCC is highly resistant to antimitotic therapies [3]. Chemotherapies (e.g. sorafenib and tivantinib) and chemotherapy in combination with radiation (e.g. RT-Sorafenib) are the most commonly applied protocols in HCC patients [4,5]. However, these therapies have severe side effects which impair life quality of the patients and may lead to interruption of the treatment [6-9].

Preprints (www.preprints.org) | NOT PEER-REVIEWED | Posted: 29 January 2021 doi:10.20944/preprints202101.0603.v1

Radiotherapy is rarely used in the management of the HCC due to lacking trail data which supports the safety and efficacy of the radiotherapy and the increased risk of radiation-induced liver damage (RILD) which follows the hepatic radiotherapy [10,11]. Thus, an important question is whether the application of chronotherapy might improve the efficacy of radiotherapy for HCC.

In a recent study with a mouse model of HCC (double transgenic c-myc/TGFα mice), we have shown significant time of day-dependent differences in proliferation rate as well as DNA damage and repair mechanisms between the HCC and the surrounding healthy liver (HL) [12]. These results suggest that the efficacy and side effects of any antimitotic therapy for HCC may depend on proper timing and that determination of the optimal time point for application of antimitotic therapies may help to improve the efficacy of HCC treatment. Such a chronotherapeutic approach has been taken in humans for other tumors such as bone and brain metastases, breast, rectal and cervical cancers but not for HCC [13]. To test the potential value of a chronotherapeutic approach, we investigated the effect of irradiation at four different *Zeitgeber* time (ZT) points in mice bearing HCCs. As an experimental animal model, *Per2::luc* mice were selected based on previous studies [14]. In order to evaluate the response to radiotherapy, Ki67 was used as a marker for proliferation and γ-H2AX as a marker for DNA-double strand breaks (DSBs) in HCC and HL. Ki67 is expressed during the G2/M phase of the cell cycle, which is the most critical target phase for radiotherapy [15,16]. In HCC, the expression of Ki67 is established as an indicator for the response to antimitotic drugs (e.g. tivantinib) [5]. In addition, it is well known that during proliferation cells become more sensitive to DNA damage induced by cancer therapies [17,18]. Thus, γ-H2AX, a histone which accumulates in the damaged sites of DNA-DSBs to start the DNA repair process [19,20], is used as an indicator for the sensitivity of tumors and the surrounding healthy tissues to the treatment protocols and helps to control the dose and the efficacy of radiotherapy [19]. In HCC, γ-H2AX was recently used as a marker to predict the efficacy of a combined sorafenib treatment with radiation (RT-SOR) and indolylquinoline derivative substances [4,21].

In contrast to experiments with whole animals, the usage of organotypic slice cultures (OSC) allows a faster and more effective screening of any novel therapeutic strategy and also improves animal welfare. In our previous study, we concluded that OSC from HCC and HL may be helpful model to test and establish novel therapeutic

Preprints (www.preprints.org) | NOT PEER-REVIEWED | Posted: 29 January 2021 doi:10.20944/preprints202101.0603.v1

strategies [12]. To investigate whether OSC is suitable to determine the optimal time points of radiotherapy, OSC slices were irradiated with two different doses (2 and 10 Gy) at 4 different circadian time (CT) points and Ki67 and γ-H2AX immunoreactive cells were analyzed.

Cell cycle, proliferation rate and DNA damage repair mechanism as well as the sensitivity to antimitotic treatments are controlled by the molecular clockwork [22-25] which is based on clock genes that interact through positive and negative transcription-translation feedback loops [26,27]. The transcription factors CLOCK and BMAL1 represent the positive elements in the loops and activate the expression of *Per* (*Per1* and *Per2*) and *Cry* (*Cry1* and *Cry2*) genes which form PER/CRY complexes representing the negative elements [27]. This molecular clockwork controls the expression of more than 3000 so-called clock-controlled genes and, thus, rhythmic cell and organ functions. Disruption of the molecular clockwork or down-regulation of clock gene expression leads to genomic instability which increases the cellular proliferation rate and thus promotes carcinogenesis [3,9,28]. In our previous study, expression of *Per2* and *Cry1* was significantly lower and showed an altered rhythm in HCC [12]. To date, little is known about the effects of radiotherapy on the molecular clockwork. Therefore, we analyzed whether radiotherapy at different ZTs affects the molecular clockwork in HCC and HL.

Hematopoiesis is one of the most sensitive systems in the body to radiotherapy and reduction of white and red blood cells is one of the most common side effects of the radiotherapy [29,30]. Thus, blood cells of mice with HCC with and without irradiation at different ZTs were analyzed as an additional readout for the side effects of the radiotherapy.

Results

Ki67 and γ-H2AX in OSCs of HCC and HL without and with irradiation with two different doses at four different CTs (*in vitro*)

In non-irradiated OSCs, the number of Ki67+ cells was very low and not different among the four CTs in HL ($p > 0.05$, Fig. 1A, C). In HCC, the number of Ki67+ cells was significantly higher ($p < 0.0001$) as compared with HL and showed a peak at CT02 which, however, did not differ from the values at the other CTs ($p > 0.05$, Fig. 1B, D).

Preprints (www.preprints.org) | NOT PEER-REVIEWED | Posted: 29 January 2021 doi:10.20944/preprints202101.0603.v1

Irradiation with 2 or 10 Gy had no effect on the number of Ki67+ cells at all CTs in HL ($p > 0.05$, Fig. 1A, C). In HCC, irradiation with 2 Gy elicited no changes in the number of Ki67+ cells at any CT ($p > 0.05$, Fig. 1B, D). In contrast, after irradiation with a dose of 10 Gy at CT02, the number of Ki67+ cells was significantly lower as compared with the respective non-irradiated HCC ($p < 0.05$). Irradiation with 10 Gy had no effect on the number of Ki67+ cells at any other time point (Fig. 1B, D).

Preprints (www.preprints.org) | NOT PEER-REVIEWED | Posted: 29 January 2021 doi:10.20944/preprints202101.0603.v1

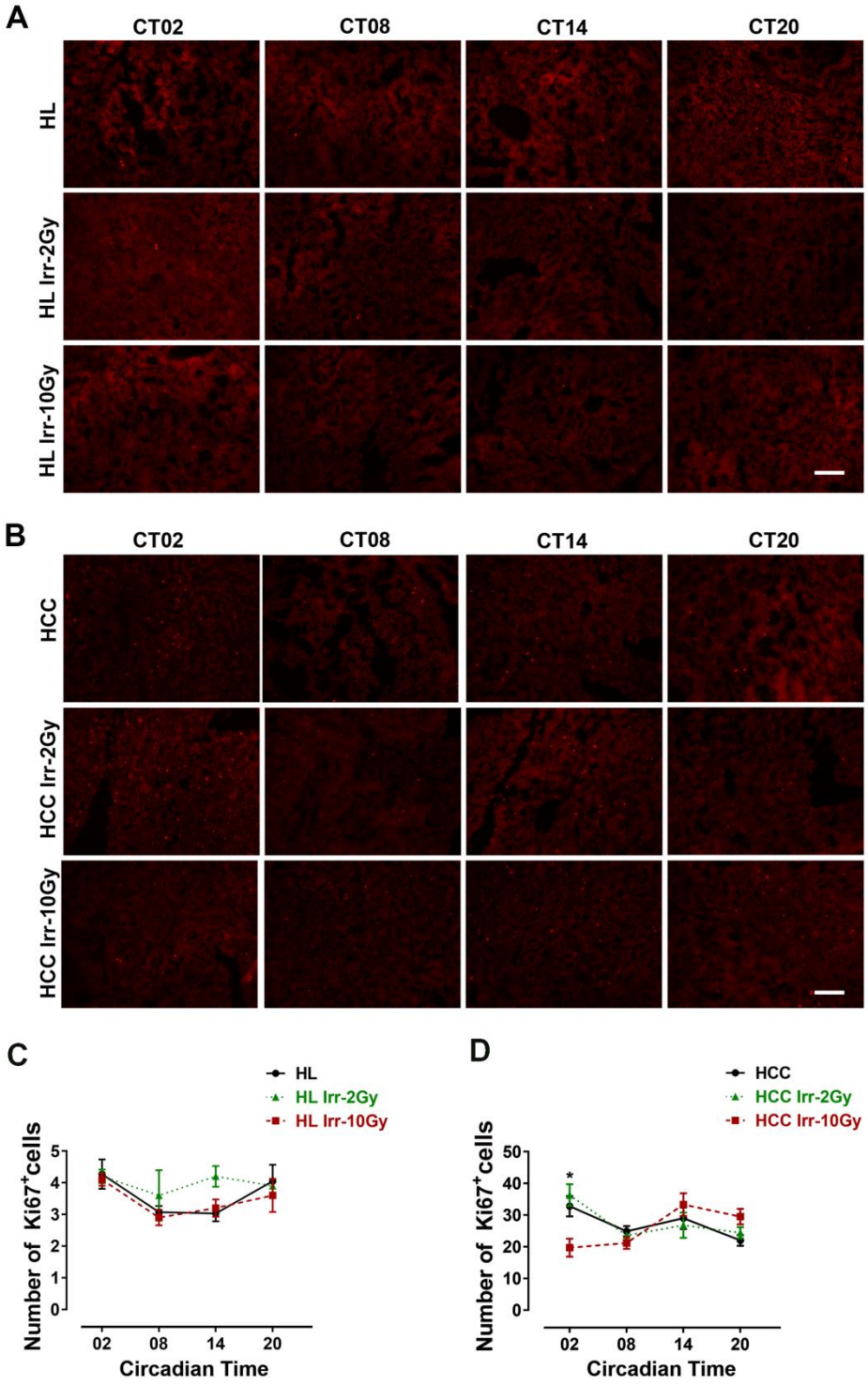

Fig. 1 Ki67 in organotypic slice cultures (OSCs) of hepatocellular carcinoma (HCC) and surrounding healthy liver (HL) with or without irradiation. At different circadian times (CT00= medium change), OSCs were irradiated (Irr) with a dose of 2 Gy or 10 Gy (n=5/time point in each dose) or handled similarly but not irradiated. 48 hours later, OSCs were collected at the same CTs. Representative photomicrographs of Ki67 immunoreaction in HL (**A**) and HCC (**B**). Quantification of Ki67 immunoreactive (+) cells in HL (**C**) and HCC (**D**). Plotted are the mean numbers ± SEM of immunoreactive (+) cells. *: $p < 0.05$ differences between the non-irradiated and irradiated OSCs with a dose of 10 Gy. Scale bars, 100 μm.

Preprints (www.preprints.org) | NOT PEER-REVIEWED | Posted: 29 January 2021 doi:10.20944/preprints202101.0603.v1

In non-irradiated HL, the number of γ-H2AX+ cells was low and showed a peak at CT02 (Fig. 2C). In HCC, the number of γ-H2AX+ cells was significantly higher in the HCC as compared with HL (Fig. 2B, D, $p < 0.0001$), and higher at CT14 ($p < 0.05$) and CT20 ($p < 0.01$) as compared with CT08 (Fig. 2D).

In HL, irradiation with either 2 or 10 Gy resulted in a time-dependent increase in the number of γ-H2AX+ cells (Fig. 2A, C). The strongest effects were observed at CT02 (39.3% and 60.2%, respectively) and CT14 (24% and 27.7%, respectively) ($p < 0.0001$). A smaller effect of irradiation with 2 and 10 Gy was observed at CT08 with a significant increase of 18.4% and 14.5%, respectively ($p < 0.01$). Irradiation at CT20 had no effect on the number of γ-H2AX+ cells ($p > 0.05$). In HCC, the number of γ-H2AX+ cells was further increased after irradiation with 2 or 10 Gy at CT02 (24.8% and 58.4%, respectively) and CT08 (19.3% and 20.2 %, respectively) as compared with non-irradiated HCC ($p < 0.0001$). At CT14, only irradiation with 10 Gy resulted in a significant increase in the number of γ-H2AX+ cells as compared with non-irradiated HCC (17%, $p < 0.001$). At CT20, irradiation had no effect on the number of γ-H2AX+ cells ($p > 0.05$, Fig. 2B, D).

Preprints (www.preprints.org) | NOT PEER-REVIEWED | Posted: 29 January 2021 doi:10.20944/preprints202101.0603.v1

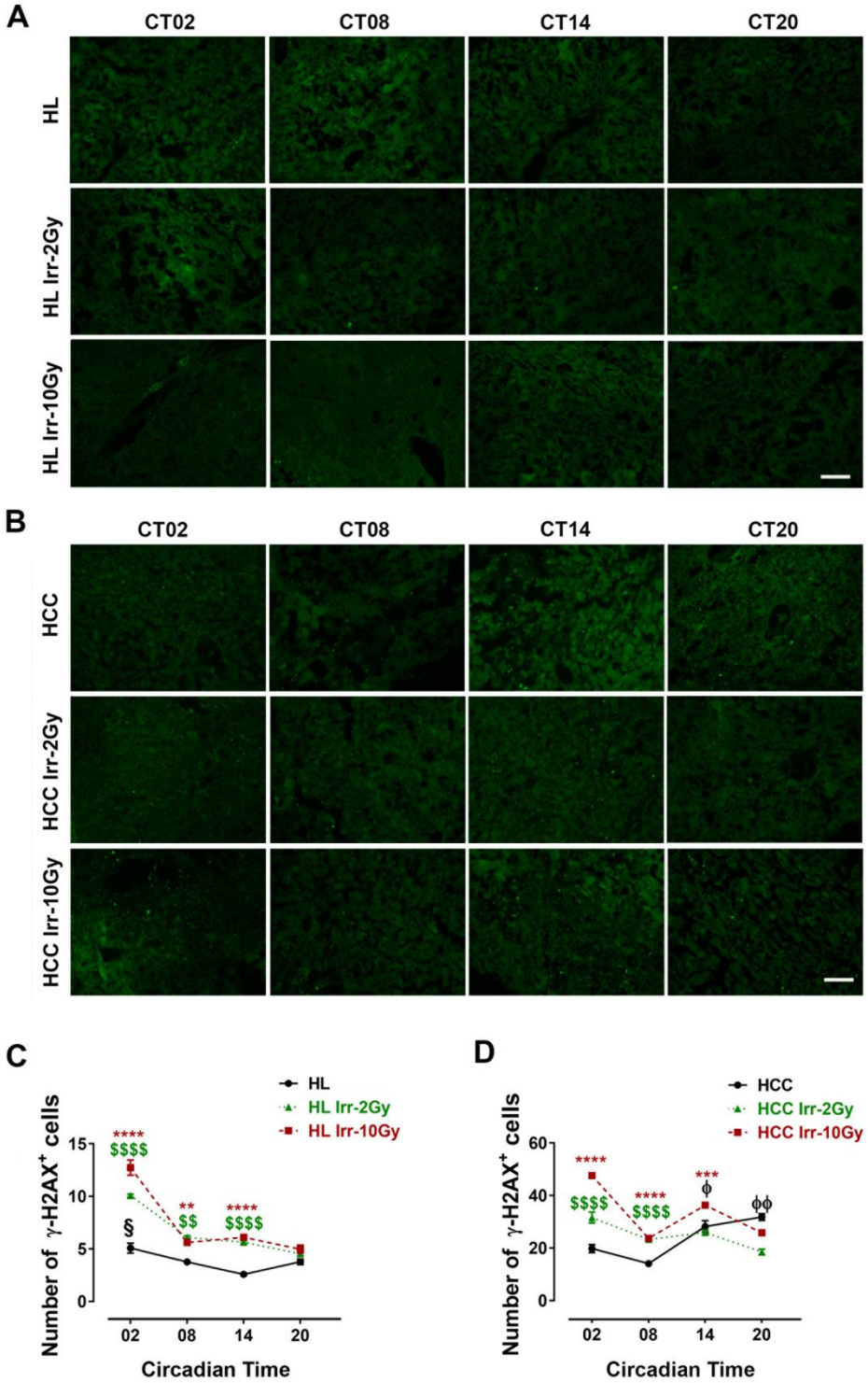

Fig. 2 γ-H2AX in organotypic slice cultures (OSCs) of hepatocellular carcinoma (HCC) and surrounding healthy liver (HL) with or without irradiation. At different circadian times (CT00= medium change), OSCs were irradiated (Irr) with a dose of 2 Gy or 10 Gy (n=5/time point in each dose) or handled similarly but not irradiated. 48 hours later, OSCs were collected at the same CTs. Representative photomicrographs of γ-H2AX immunoreaction in HL (**A**) and HCC (**B**). Quantification of γ-H2AX immunoreactive (+) cells HL (**C**) and HCC (**D**). Plotted are the mean numbers ± SEM of immunoreactive (+) cells. §: *p <0.05* differences between this CT and CT14. φ: *p <0.05*; φφ: *p <0.01* differences between this CT and CT08.**: *p <0.01*; ***: *p <0.001*; ****: *p <0.0001* differences between the non-irradiated and irradiated OSCs with a dose of 10 Gy. $$: *p <0.01*; $$$$: *p <0.0001* differences between the non-irradiated and irradiated OSCs with a dose of 2 Gy. Scale bars, 100 μm.

Preprints (www.preprints.org) | NOT PEER-REVIEWED | Posted: 29 January 2021 doi:10.20944/preprints202101.0603.v1

Ki67 and γ-H2AX in HCC and HL in mice without and with irradiation (10 Gy) at four different ZTs (*ex vivo*)

In non-irradiated HL, the number of Ki67+ cells showed one peak during the light phase (ZT02) which was significantly different from the trough at the early dark phase (ZT14, $p < 0.001$) (Fig. 3A, C). In HCC, the number of Ki67+ cells was higher than in HL at all ZTs (ZT02, 14, 20, $p < 0.0001$; ZT08, $p < 0.01$), but in contrast to the HL, the number of Ki67+ cells showed two peaks, one during the early light phase (ZT02, $p < 0.05$) and the second in the late dark phase (ZT20, $p < 0.01$) as compared with the trough at ZT08 (Fig. 3D).

Irradiation (10 Gy) resulted in a decrease in the number of Ki67+ cells. In HL, the highest effect of irradiation was observed after irradiation during the light phase, when Ki67 expressions were high without irradiation (ZT02, 89.8%; ZT08, 60.6%, $p < 0.0001$). During the dark phase, when Ki67 expression was low without irradiation, irradiation had little (ZT20, 32.6 %, $p < 0.05$) or no (ZT14) effect (Fig. 3A, C). In HCC, irradiation resulted in a significant decrease in Ki67+ cells at all ZTs (ZT02, 72.3%; ZT08, 37.7%; ZT14, 67.1%; with the strongest decrease observed at ZT20, 94.3%) (Fig. 3B, D).

Preprints (www.preprints.org) | NOT PEER-REVIEWED | Posted: 29 January 2021 doi:10.20944/preprints202101.0603.v1

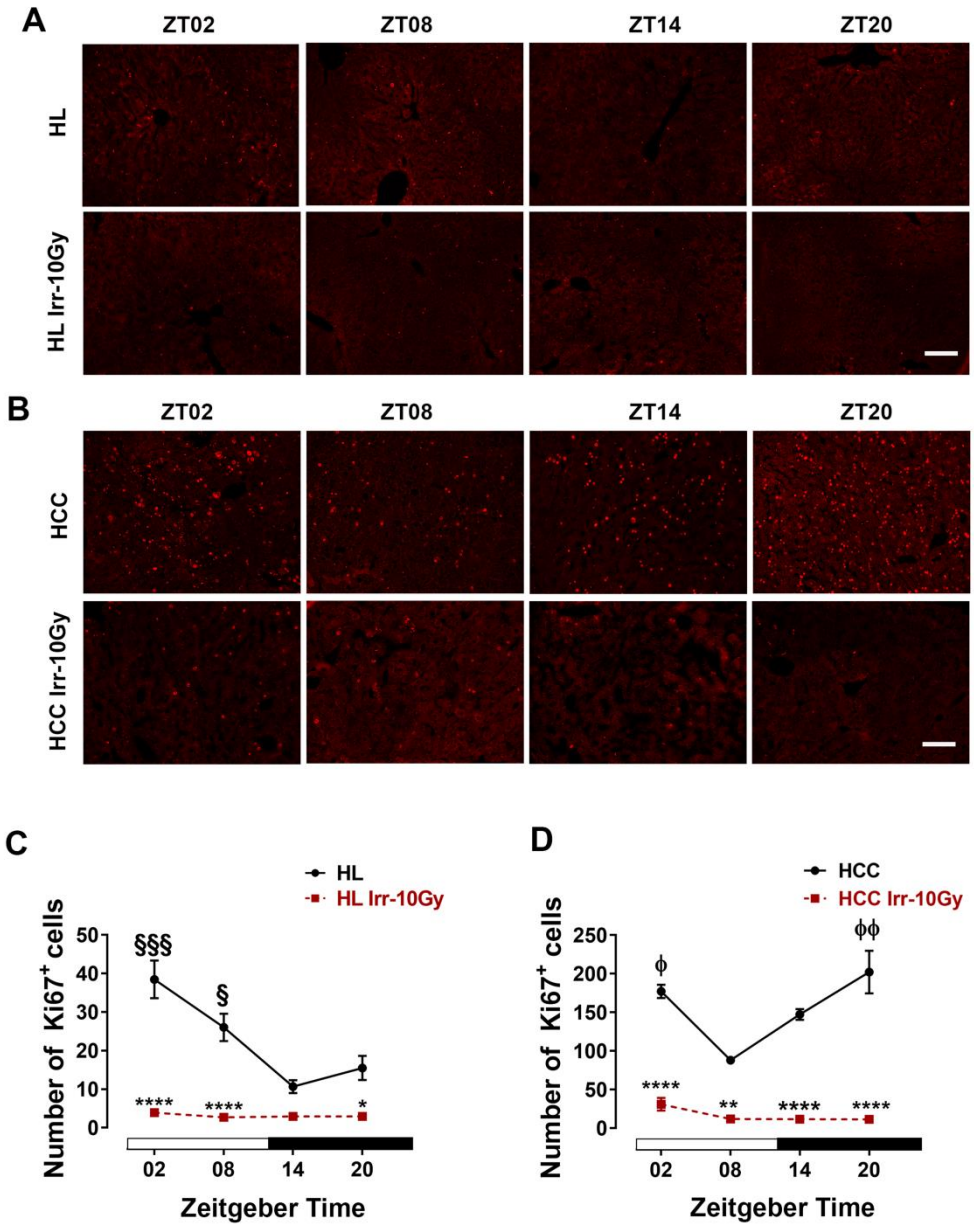

Fig. 3 Ki67 in *ex vivo* samples of hepatocellular carcinoma (HCC) and healthy liver (HL) with or without irradiation. At different *Zeitgeber* times (ZT00= the onset of the light phase), mice were irradiated (Irr-10Gy) (n= 3/time point) or handled similarly but not irradiated. 48 hours later, mice were sacrificed at the same ZTs. Representative photomicrographs of Ki67 immunoreaction in HL (**A**) and HCC (**B**). Quantification of Ki67 immunoreactive (+) cells in HL (**C**) and HCC (**D**). Plotted are the mean numbers ± SEM of immunoreactive (+) cells. White and black bars indicate the light and dark phases, respectively. §: $p < 0.05$; §§§: $p < 0.001$ differences between this ZT and ZT14. φ: $p < 0.05$; φφ: $p < 0.01$ differences between this ZT and ZT08. *: $p < 0.05$; **: $p < 0.01$; ****: $p < 0.0001$ differences between the non-irradiated and irradiated group. Scale bars, 100 μm.

Preprints (www.preprints.org) | NOT PEER-REVIEWED | Posted: 29 January 2021 doi:10.20944/preprints202101.0603.v1

In non-irradiated HL, the number of γ-H2AX+ cells showed a peak in the early light phase (ZT02) which was significantly different from the trough at the early dark phase (ZT14) ($p < 0.0001$, Fig. 4A, C). In non-irradiated HCC, the number of γ-H2AX+ cells was significantly higher at ZT02 and ZT20 ($p < 0.0001$) as compared with HL. The HCC revealed two peaks, one at ZT02 and a second at ZT20. The two peaks were significantly different from the minimum at ZT08 ($p < 0.05$, Fig. 4D).

Irradiation led to an increase in the number of γ-H2AX+ cells at all four ZTs in HCC and HL as compared with non-irradiated samples. As compared with non-irradiated HL, the number of γ-H2AX+ cells in HL was higher when the animals were irradiated at ZT02 and ZT14 (90.7% and 80%, respectively; $p < 0.0001$) than at ZT08 (47.9%, $p < 0.001$) and ZT20 (32.2%, $p < 0.05$; Fig. 4A, C and Fig. S1). In irradiated HCC, the number of γ-H2AX+ cells was significantly increased ($p < 0.01$) as compared with the non-irradiated HCC at all ZTs (Fig. 4B, D).

Preprints (www.preprints.org) | NOT PEER-REVIEWED | Posted: 29 January 2021 doi:10.20944/preprints202101.0603.v1

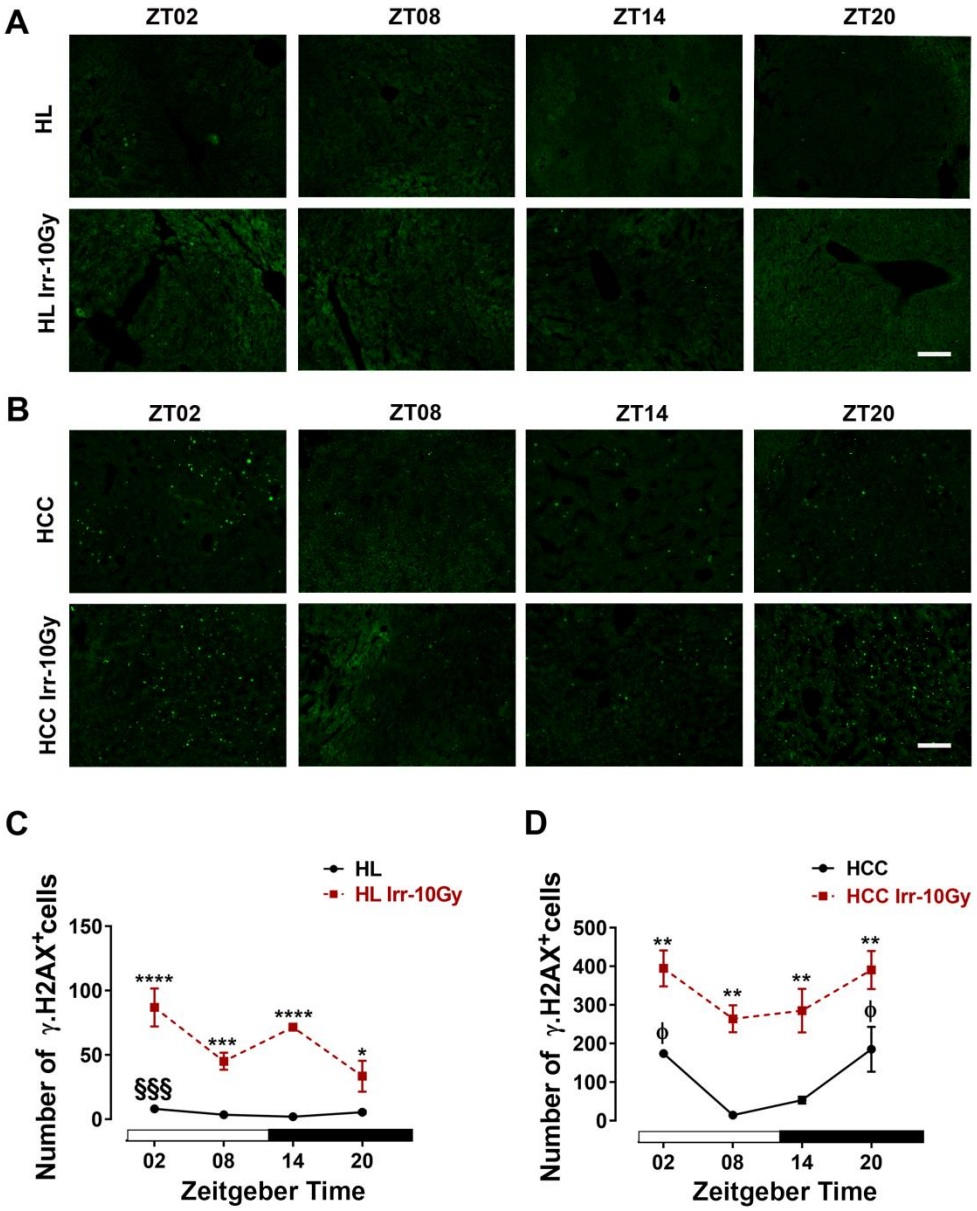

Fig. 4 γ-H2AX in *ex vivo* samples of hepatocellular carcinoma (HCC) and healthy liver (HL) with or without irradiation. At different *Zeitgeber* times (ZT00= the onset of the light phase), mice were irradiated (Irr-10Gy) (n= 3/time point) or handled similarly but not irradiated. 48 hours later, mice were sacrificed at the same ZTs. Representative photomicrographs of γ-H2AX immunoreaction in HL (**A**) and HCC (**B**). Quantification of γ-H2AX immunoreactive (+) cells in HL (**C**) and HCC (**D**). Plotted are the mean numbers ± SEM of immunoreactive (+) cells. White and black bars indicate the light and dark phases, respectively. §§§: $p < 0.001$ differences between this ZT and ZT14. φ: $p < 0.05$ differences between this ZT and ZT08. *: $p < 0.05$; **: $p < 0.01$; ***: $p < 0.001$; ****: $p < 0.0001$ differences between the non-irradiated and irradiated group. Scale bars, 100 μm.

Preprints (www.preprints.org) | NOT PEER-REVIEWED | Posted: 29 January 2021 doi:10.20944/preprints202101.0603.v1

Clock gene expression in HCC and HL in mice without and with irradiation (10 Gy) at four different ZTs (*ex vivo*)

The relative expression of *Per1* in non-irradiated HL and HCC showed a peak at ZT14 which was significantly different from the value at ZT02 ($p < 0.05$). There were no differences between HCC and HL among ZTs ($p > 0.05$). The relative expression of *Per1* did not differ when the irradiated HL and HCC were compared with the non-irradiated samples at all irradiated ZTs ($p > 0.05$, Fig. 5A, B).

The relative expression of *Per2* in non-irradiated HL and HCC was higher at ZT14 and ZT20 as compared with ZT08 ($p < 0.05$). At ZT02, the relative expression of *Per2* was lower in HCC than in HL ($p < 0.05$). When the mice were irradiated at ZT14, the relative expression of *Per2* was significantly increased in both the HL and the HCC ($p < 0.001$; $p < 0.01$, Fig. 5C, D).

The relative expression of *Cry1* showed a peak at ZT02 in non-irradiated HL which was significantly different from the value at ZT14 ($p < 0.05$, Fig. 5E). In non-irradiated HCC, the relative expression of *Cry1* was not different among the ZTs (Fig. 5F) and was significantly lower as compared with non-irradiated HL at ZT02 ($p < 0.01$). Irradiation had no effect on the relative expression of *Cry1* in HCC or HL ($p > 0.05$, Fig. 5E, F).

The relative expression of *Cry2* was not different among the ZTs in HL or HCC (Fig. 5G, H). At ZT02, the relative expression of *Cry2* was lower in HCC than in HL ($p < 0.01$). When the mice were irradiated at ZT14, the relative expression of *Cry2* was increased in HCC as compared with the non-irradiated HCC ($p < 0.05$, Fig. 5H).

Preprints (www.preprints.org) | NOT PEER-REVIEWED | Posted: 29 January 2021 doi:10.20944/preprints202101.0603.v1

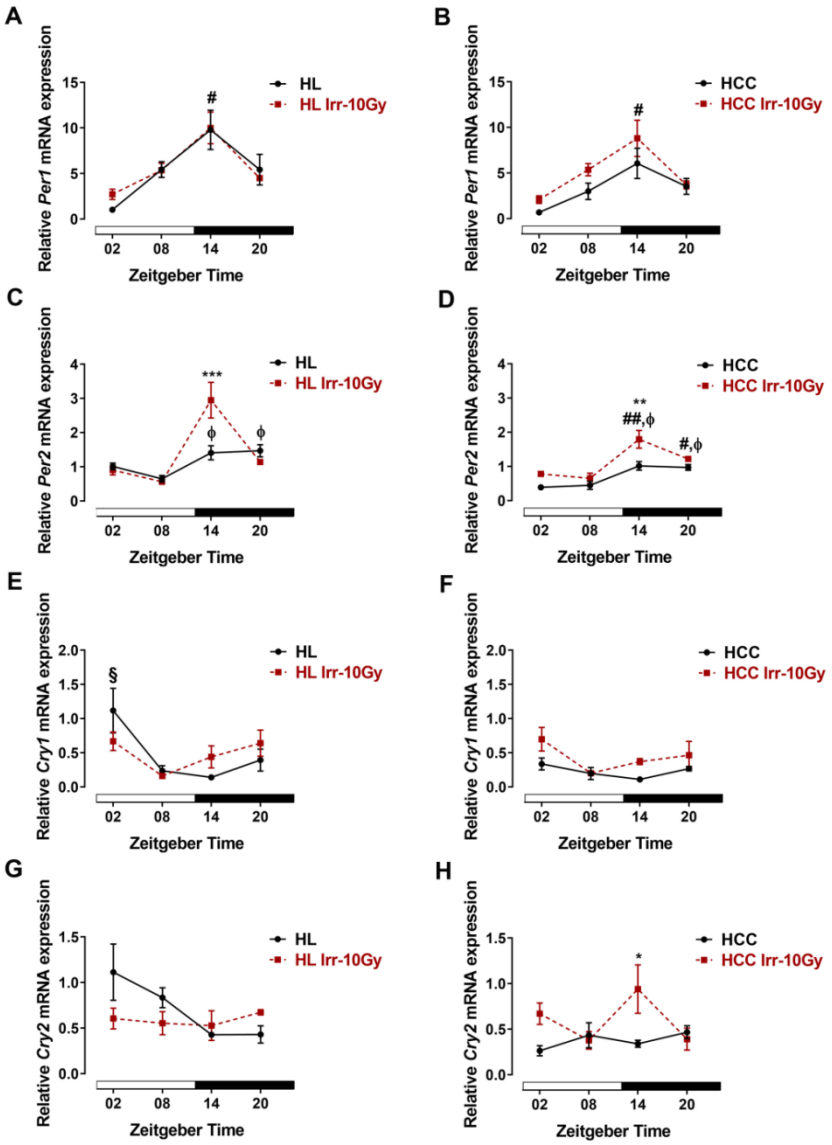

Fig. 5 Clock gene expressions in *ex vivo* samples of hepatocellular carcinoma (HCC, left panel) and surrounding healthy liver (HL, right panel) without or with irradiation (Irr-10Gy). At different *Zeitgeber* times (ZT00= the onset of the light phase), mice were irradiated (n= 3/time point) or handled similarly but not irradiated. 48 hours later, mice were sacrificed at the same ZTs. Relative expression of *Per1* in HL (**A**) and HCC (**B**). Relative expression of *Per2* in HL (**C**) and HCC (**D**). Relative expression of *Cry1* in HL (**E**) and HCC (**F**). Relative expression of *Cry2* in HL (**G**) and HCC (**H**). Plotted are the mean relative mRNA expressions ± SEM. White and black bars indicate the light and dark phases, respectively. #: $p < 0.05$; ##: $p < 0.01$ differences between this ZT and ZT02. φ: $p < 0.05$ differences between this ZT and ZT08. §: $p < 0.05$ differences between this ZT and ZT14. *: $p < 0.05$; **: $p < 0.01$; ***: $p < 0.001$ differences between the non-irradiated and irradiated group.

Preprints (www.preprints.org) | NOT PEER-REVIEWED | Posted: 29 January 2021 doi:10.20944/preprints202101.0603.v1

The relative expression of *Clock* in non-irradiated HL showed a peak at ZT08 which was significantly different from ZT14 and ZT20 ($p < 0.05$, Fig. 6A). In non-irradiated HCC, the relative expression of *Clock* was not different among the ZTs ($p > 0.05$, Fig. 6B) and was lower at ZT02 ($p < 0.01$) and ZT08 ($p < 0.001$) as compared with HL. In HL irradiated at ZT02 ($p < 0.01$) and ZT08 ($p < 0.001$), the relative expression of *Clock* was reduced as compared with the non-irradiated HL (Fig. 6A).

The relative expression of *Bmal1* in non-irradiated HL showed a peak at ZT02 which was significantly different from ZT14 ($p < 0.01$) and ZT20 ($p < 0.05$, Fig. 6C). In non-irradiated HCC, the relative expression of *Bmal1* was not different among the ZTs ($p > 0.05$, Fig. 6B) and was lower at ZT02 as compared with HL ($p < 0.01$). After irradiation at ZT02, the relative expression of *Bmal1* was decreased in irradiated HL and increased in HCC as compared with non-irradiated samples ($p < 0.05$, Fig. 6C, D).

The relative expression of *Rev-erbα* showed a peak at (ZT08) in non-irradiated HL ($p < 0.001$) and HCC ($p < 0.05$) which differed from ZT20 (Fig. 6E, F). At ZT08, the relative expression of *Rev-erb α* was lower in HCC than in HL ($p < 0.0001$). Irradiation of the mice had no effect on the relative expression of *Rev-erbα* ($p > 0.05$, Fig. 6E, F).

Preprints (www.preprints.org) | NOT PEER-REVIEWED | Posted: 29 January 2021 doi:10.20944/preprints202101.0603.v1

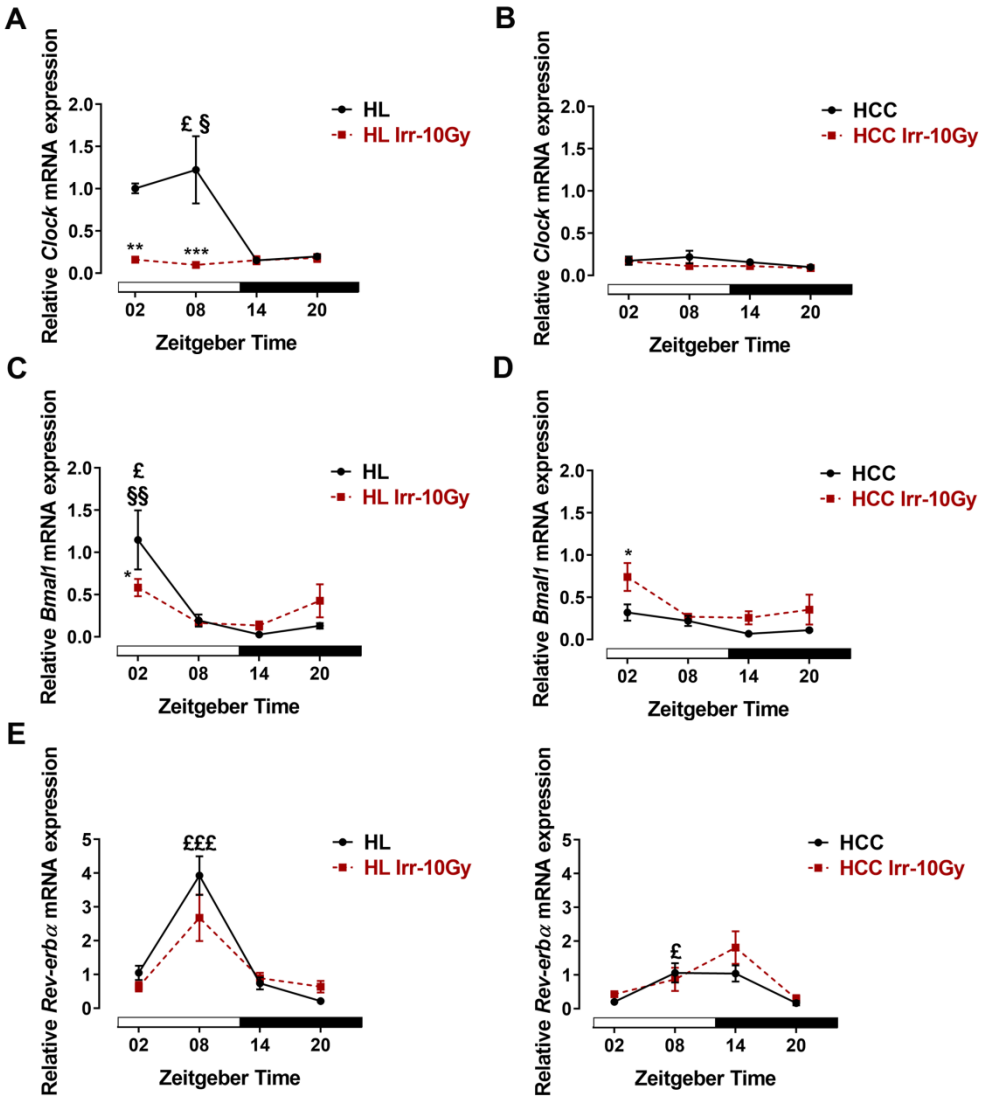

Fig. 6 Clock gene expressions in *ex vivo* samples of hepatocellular carcinoma (HCC, left panel) and healthy liver (HL, right panel) without or with irradiation (Irr-10Gy). At different *Zeitgeber* times (ZT00= the onset of the light phase), mice were irradiated (n= 3/time point) or handled similarly but not irradiated. 48 hours later, mice were sacrificed at the same ZTs. Relative expression of *Clock* in HL (**A**) and HCC (**B**). Relative expression of *Bmal1* in HL (**C**) and HCC (**D**). Relative expression of *Rev-erbα* in HL (**E**) and HCC (**F**). Plotted are the mean relative mRNA expressions ± SEM. White and black bars indicate the light and dark phases, respectively. §: $p < 0.05$; §§: $p < 0.01$ differences between this ZT and ZT14. £: $p < 0.05$; £££: $p < 0.001$ differences between this ZT and ZT20. *: $p < 0.05$; **: $p < 0.01$; ***: $p < 0.001$ differences between the non-irradiated and irradiated group.

Preprints (www.preprints.org) | NOT PEER-REVIEWED | Posted: 29 January 2021 doi:10.20944/preprints202101.0603.v1

Blood cell counts in mice without and with irradiation (10 Gy) at four different ZTs (*ex vivo*)

Control mice showed a daily variation in the total number of leukocytes with higher levels during the light phase than during the dark phase (Fig. 7A). In the non-irradiated HCC group, there was no significant daily variation of leukocytes and at ZT20 the leukocytes number was significantly higher as compared with the control group ($p < 0.05$, Fig. 7A). In the irradiated group, the number of leukocytes at ZT02 ($p < 0.05$) and ZT08 ($p < 0.01$) was significantly decreased (Fig. 7A).

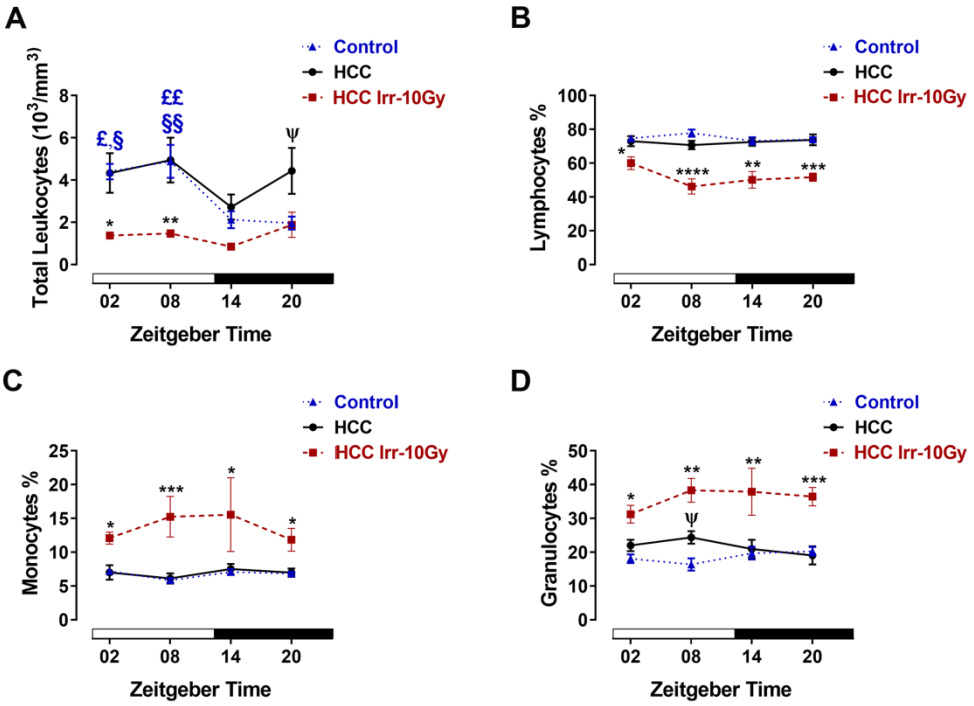

Fig. 7 Blood cell analysis in control and hepatocellular carcinoma (HCC) bearing mice without and with irradiation. At different *Zeitgeber* times (ZT00= the onset of the light phase), mice were irradiated (Irr) with a dose of 10 Gy (n= 3-6/time point) or handled similarly but not irradiated. 48 hours later, mice were sacrificed and the blood was collected at the same ZTs. (**A**) Total leukocytes numbers. (**B**) Lymphocyte percentage. (**C**) Monocyte percentage. (**D**) Granulocyte percentage. Plotted are the mean numbers ± SEM. White and black bars indicate the light and dark phases, respectively. §: $p < 0.05$; §§: $p < 0.01$ differences between this ZT and ZT14. £: $p<0.05$; ££: $p < 0.01$ differences between this ZT and ZT20. *: $p < 0.05$; **: $p < 0.01$; ***: $p < 0.001$; ****: $p < 0.0001$ differences between non-irradiated and irradiated animals. ψ: $p<0.05$ differences between control and non-irradiated animals.

Preprints (www.preprints.org) | NOT PEER-REVIEWED | Posted: 29 January 2021 doi:10.20944/preprints202101.0603.v1

There were no differences in the percentages of leukocyte types in both the control group and the HCC mice (Fig. 7B-D). However, at ZT08, the percentage of the granulocytes was higher in HCC mice as compared with the control group ($p < 0.05$, Fig. 7D). Irradiation at any time point resulted in a decrease in percentage of lymphocytes and an increase in the percentage of both monocytes and granulocytes as compared with the non-irradiated HCC mice (Fig. 7B-D). There were no differences in the number of erythrocytes, platelets and the hemoglobin concentration in control, non-irradiated, and irradiated mice (Supplementary Figure S2 A-C).

Discussion

This study with a newly developed mouse model for hepatocellular carcinoma (HCC) addresses the question of whether timed application of radiotherapy may increase the efficacy of hepatocellular carcinoma treatment in mice which was raised from our recent findings in double transgenic c-myc/TGFα [12]. Irradiation was performed at four different time points. Readouts for treatment efficacy and side effects were proliferation, DNA-DSBs, clock gene expression and blood cell counts.

As a first step, time- and dose-dependent effects were analyzed in OSC of HL and HCC either irradiated at 4 different circadian time (CT) points (CT02, CT08, CT14 and CT20) with two different doses (2 and 10 Gy) or left without irradiation. Irradiation with 2 Gy or 10 Gy affected DNA-DSBs: as compared with the non-irradiated slices, the number of γ-H2AX+ cells was increased in both HL and HCC irradiated at CT02, 08 and 14. This indicates a similar time- and dose-dependent effect of irradiation on DNA-DSBs in healthy tissue and tumor. With regard to proliferation in non-irradiated HCC, the number of Ki67+ cells revealed two peaks (CT02 and CT14) which correspond to the two peaks previously observed also in double transgenic c-myc/TGFα mice [12]. After irradiation of HCC and HL slices with a dose of 2 Gy at the different CTs, the number of Ki67+ cells did not differ from those in the non-irradiated groups. Thus, the low dose of irradiation does not affect proliferation in HCC. In contrast, irradiation with 10 Gy elicited a strong antiproliferative effect: HCC slices irradiated with a dose of 10 Gy at CT02 (the proliferation peak) showed a decrease in the number of Ki67+ cells as compared with the non-irradiated HCC. Notably, irradiation with 10 Gy at this CT did not affect the proliferation rate in HL. Dose-dependent antiproliferative effects were also found in

Preprints (www.preprints.org) | NOT PEER-REVIEWED | Posted: 29 January 2021 doi:10.20944/preprints202101.0603.v1

other *in vitro* models of cancer. Irradiation of DU 145 cells (a human prostate cancer cell line) inhibited their proliferation only when given in high doses (10 and >20 Gy), while a dose of 2 Gy was ineffective [31]. A dose of 10 Gy was also shown to cause disruption in the mitotic stage and initiation of cell apoptosis in HeLa cells, a cervical cancer cell line [32].

Since the *in vitro* data showed antiproliferative effects of irradiation only at a dose of 10 Gy, we used this dose for our *ex vivo* analyses with whole animals which were irradiated at 4 different *Zeitgeber* time (ZT) points (ZT02, ZT08, ZT14 and ZT20) or left without irradiation. As in OSC, the number of Ki67+ cells was much higher in non-irradiated HCC than in HL. Both tissues showed a daily variation in the number of Ki67+ cells but the pattern was different. The non-irradiated HL showed one peak at ZT02, whilst the non-irradiated HCC showed two peaks, a maximum at the late activity phase (ZT20) and a second peak in the early inactivity phase (ZT02). This is in contrast to the time course in OSCs. Two proliferation peaks were also observed in double transgenic c-myc/TGFα [12] and thus seem to be a characteristic feature of fast-growing tumors [33,34]. A difference in proliferation peaks between tumor and surrounding healthy tissue was also observed in other tumors [35,36]. The daily variations of cell proliferation in HCC and the HL result from the circadian oscillation of the cell cycle molecules which either promote or inhibit cell cycle proliferation (e.g. CycD1 and c-Myc) [33,36,37].

Irradiation resulted in a decrease in the number of Ki67+ cells in both HL and HCC at all-time points except in HL at ZT14, the trough of Ki67 expression. Importantly, the effect was most pronounced when the radiotherapy was applied at the time points of the proliferation peaks which were different between the HCC and HL. Notably, irradiation at ZT20 had a low antiproliferative effect on HL (32.6%) but had the highest anti-proliferative effect on the HCC (94.3%).

In the *ex vivo* samples without irradiation, the number of γ-H2AX+ cells was much higher in HCC than in HL, consistent with the *in vitro* data and with our previous findings [12]. Both tissues showed a daily variation in γ-H2AX immunoreaction. HL showed only one peak at ZT02 while HCC showed an additional peak at ZT20. The increase of γ-H2AX+ cells in HCC during the second half of the dark phase is consistent with our previous findings [12]. Notably, the time courses of

Preprints (www.preprints.org) | NOT PEER-REVIEWED | Posted: 29 January 2021 doi:10.20944/preprints202101.0603.v1

Ki67 and γ-H2AX run largely parallel in both tissues, indicating an interconnection of the two cell cycle components in both healthy tissue and tumor.

In both HCC and HL, irradiation resulted in an increase in the number of γ-H2AX+ cells. The effect of irradiation on DNA damage was time-dependent. In HL, it was highest at ZT02 and ZT14, intermediate at ZT08 and lowest at ZT20. In HCC, the effect of irradiation was similar at all ZTs. Importantly, radiotherapy treatment during the late activity phase (ZT20) had the lowest effect on DNA-DSBs damage in HL and caused effective damage in HCC. The increase in the number of γ-H2AX+ cells after irradiation confirms that the irradiation induces the DNA-DSBs repairing mechanism [38] and that X-rays as well as ionizing radiotherapy contribute to the γ-H2AX response [19].

Disruption or mutation of clock genes is associated with genomic instability and increased proliferation rate, both favorable conditions for carcinogenesis [3,28]. Thus, we analysed the expression of seven core clock genes in the HCC and the surrounding HL of non-irradiated and irradiated animals. In HL, all clock genes showed a time-dependent variation consistent with our previous observations [12]. In HCC, *Per1*, *Per2*, and *Rev-erbα* showed a similar time course, although *Rev-erbα* showed reduced amplitude, indicating that rhythmic expression of these clock genes is regulated similarly in the tumor and the healthy liver. The molecular clockwork in liver is controlled by many different rhythmic cues such as food intake, glucocorticoids, insulin and body temperature [26,27,39-41]. These rhythmic cues might also regulate the rhythmic expression of clock genes in the tumor. However, expression of the other clock genes, *Cry1*, *Cry2*, *Clock*, and *Bmal1* showed a time-dependent decrease in HCC as compared with the HL. Transcription of *Wee1* which inhibits the entry into mitosis through inhibiting Cdk1, a key player in cell cycle regulation, is activated by CLOCK/BMAL1 and repressed by PER/CRY [42]. Thus, down-regulation of *Cry1*, *Cry2*, *Clock* and *Bmal1* might be linked with the enhanced proliferation in HCC. Clock gene expression is differently altered in various tumors [43-48] for multiple reasons. One major reason for clock gene dysregulation is a lack of tumor vascularization with many consequences such as a lack of access to circadian resetting cues in the blood and hypoxia [49]. Chronic hypoxia leads to an activation of transcription factors such as HIF-1α and HIF-1β, which bind to hypoxia response elements in the promoter region of target genes [49,50]. In the HCC cell line,

Preprints (www.preprints.org) | NOT PEER-REVIEWED | Posted: 29 January 2021 doi:10.20944/preprints202101.0603.v1

PLC/PRF/5, experimental hypoxia led to altered clock gene expression [51]. In addition, hyper-methylation of clock gene promoter regions is discussed as possible reasons for clock gene dysregulation in tumors [47,49,51].

To date, little is known about the effects of radiotherapy on the molecular clockwork which controls several rhythmic cell functions and thus affecting tolerability and efficacy of anticancer treatments [6,52,53]. Clock genes regulate DNA damage checkpoint responses, DNA repair mechanisms, and apoptosis in response to ionizing radiation in the healthy tissue [54]. Mice with mutations/deletion in the clock genes, *Clock/Bmal1* and *Per1/2*, showed enhanced chemotherapy- or gamma radiation-induced toxicity in the healthy tissue [55,56] and *Per2* mutant mice are more prone to develop cancer induced by gamma radiation or chronic nitrosamine treatment [36,44]. An effect of gamma irradiation on clock gene expression in liver has been reported before in OSC [14] and with the whole animals [14,36], however the experiments with the whole animals were only performed at one time point of irradiation (ZT10) and during the acute phase, up to 15 h after irradiation [36]. Most remarkably, the clock gene expression pattern in the tumor predicts the response of tumor patients to chemo-radiotherapy [53], emphasizing the role of the molecular clockwork in the efficacy of cancer treatment. Thus, we analyzed the effect of irradiation on clock gene expression in HL and HCC. In HL, irradiation resulted in a down-regulation in expression of the transcriptional activators *Clock* (ZT02, 08) and *Bmal1* (ZT02) and an up-regulation in expression of the transcriptional repressor *Per2* (ZT14). Importantly, irradiation at ZT20 had no effect on clock gene expression in HL. This is consistent with a low impact of irradiation on proliferation and DNA-DSBs in HL at this time point.

Hematopoiesis is one of the most sensitive systems in the body to radiotherapy and reduction of white and red blood cells are one of the most common side effects of radiotherapy [29,30]. Thus, we analyzed the number of blood cells in control and HCC bearing mice with and without irradiation at different ZTs to monitor time-dependent acute side effects of radiotherapy.

The control mice showed significant daily variations in the number of leukocytes with a peak at the light phase and a trough at the dark phase while the number of erythrocytes and the hemoglobin concentration was not significantly

Preprints (www.preprints.org) | NOT PEER-REVIEWED | Posted: 29 January 2021 doi:10.20944/preprints202101.0603.v1

different among time points. This is consistent with an earlier study in C57BL/6 mice [57]. In HCC bearing mice, the number of leukocytes was increased during the late dark phase (ZT20) and the percentage of granulocytes was increased at ZT08. Our previos data (submitted paper [58]) showed that corticosterone levels are increased at ZT08 in the HCC bearing mice. Glucocorticoids are known to increase granulocytosis [59]. Thus, the increase in glucocorticoids may account for the change in leukocyte number and composition. While irradiation had no effect on hemoglobin concentration, erythrocyte or platelet numbers, it caused a significant reduction in the total number of leukocytes. Irradiation when applied at ZT02 and ZT08 caused a significant depletion in the total number of leukocytes conforming to data on white blood cell counts in patients [60,61]. Notably, irradiation at ZT14 and ZT20 had no effect on the total leukocyte number, thus, these time points might be preferable for radiotherapy in terms of reducing this severe side effect.

Irrespective of the time of irradiation, the percentage of lymphocytes was significantly decreased, while the percentage of the other types of leucocytes were increased. Consistently, antimitotic therapy led to a dramatic decrease in the number of circulating lymphocytes independent of a functional molecular clockwork [55]. We could find recently, that irradiation of HCC bearing mice resulted in a strong increase in corticosterone levels (submitted paper [58]). Lymphocyte apoptosis is enhanced by glucocorticoids [62,63] and the decrease in lymphocytes might be a consequence of increased corticosterone levels after irradiation recently demonstrated (submitted paper [58]). In contrast, the increased percentages of granulocytes and monocytes, which build the first line of defense during the inflammation, may be due to the release of the proinflammatory cytokines (e.g. IL-1 and TNF-α), chemokines (e.g. IL-8) and factors participating in the early inflammatory response to the radiation [60,64,65].

As expected, no effect was observed in number of erythrocytes 2 days after irradiation because of the fact that the erythrocytes survive for 120 days and the reduction in number of erythrocytes after radiotherapy is considered one of the long-term side effects.

Preprints (www.preprints.org) | NOT PEER-REVIEWED | Posted: 29 January 2021 doi:10.20944/preprints202101.0603.v1

Material and method

Experimental animals and HCC induction

Male transgenic *Per2::luc* mice on a C57BL6/J background were used according to accepted standards of humane animal care and federal guidelines and Directive 2010/63/EU of the European Union. All experiments were approved by the Regierungspräsidium Darmstadt and the Landesamt für Natur, Umwelt und Verbraucherschutz NRW (Reference number: AZ 81-02.04.2018-A146). At the age of 2 weeks, the mice were injected intraperitoneally with a single dose of diethylnitrosamine (DEN) (10 mg/kg body weight, Sigma Aldrich, St. Louis, USA) to induce HCC. Phenobarbital (PB) (Luminal, Desitin, Hamburg, Germany) was chronically administered via the drinking water with a concentration of 0.05% to accelerate the HCC induction. Food and water containing PB were supplied ad libitum. All mice were kept under the standard light-dark (LD) cycle (12:12). ZT00 defines the onset of the light phase. All experiments during the dark phase were performed under dim red light. At the age of 7-10 months, HCC presented either as a single big tumor or as multiple smaller tumors (Supplementary Figure S3). Tumor development was screened via magnetic resonance imaging and post mortem inspection.

Magnetic resonance imaging (MRI)

For MRI, mice were anesthetized with 1.5% isoflurane in a water-saturated gas mixture of 20% oxygen in nitrogen applied at a rate of 75 mL/min by manually restraining the animal and placing its head in an in-house-built nose cone. Respiration was monitored with a pneumatic pillow positioned at the animal's back. Vital function was acquired by using an M1025 system (SA Instruments, Stony Brook, NY) to synchronize data acquisition with respiratory motion. Throughout the experiments mice were breathing spontaneously at a rate of ~100 min-1 and were kept at 37 °C. Animals were placed within the resonator so that in z-direction (30 mm) the field of view (FOV) covered the abdomen from just below the diaphragm down to the pelvis.

Data were recorded on a Bruker AvanceIII 9.4 Tesla Wide Bore (89 mm) nuclear magnetic resonance (MR) spectrometer (Bruker, Rheinstetten, Germany) operating at a frequency of 400.13 MHz for 1H. Experiments were carried out using a Bruker microimaging unit (Micro 2.5) equipped with actively shielded gradient sets

Preprints (www.preprints.org) | NOT PEER-REVIEWED | Posted: 29 January 2021 doi:10.20944/preprints202101.0603.v1

(capable of 1.5 T/m maximum gradient strength and 150 µs rise time at 100% gradient switching), a linear 1H 25-mm birdcage resonator, and Paravision 5.1 as operating software.

Liver tumors were determined by acquisition of images with a respiratory-gated 2D 1H multi-slice fast low angle snapshot (FLASH) gradient-echo sequence exploiting the native tissue contrast between healthy liver and tumor tissue (see supplementary Figure S4). Data were taken from a field-of-view of 25.6×25.6 mm^2 with a spatial resolution of 100×100 μm^2 (TE, 1.62 ms; TR, 111.52 ms; slices, 16; slice thickness, 1 mm; averages, 1, acquisition time, 15 s).

Irradiation of organotypic slice cultures (OSC)

Mice with HCC were sacrificed at ZT02. The liver was dissected under sterile conditions and stored quickly in ice-cold storage solution (MACS tissue storage solution, Miltenyi Biotec, Bergisch Gladbach, Germany). HL and HCCs were sliced separately into 600µm thick sections using a Krumdieck tissue chopper (TSE Systems, Bad Homburg, Germany) and kept in ice-cold sterilized Dulbecoo's phosphate buffered saline (DPBS) (Gibco by Life Technologies, Paisley, UK). Then the slices were transferred to cell culture inserts (0.4 µm pores, Falcon, Durham, USA) which were inserted in 6 well plates filled with 1 ml pre-warmed culture medium modified according to previously published protocol [66]. The medium consisted of DMEM, supplemented with 10% fetal bovine serum, 100 U/ml penicillin, 0.1 mg/ml streptomycin, 10 mmol/l HEPES, 1 mg/ml insulin, 8 mg/ml ascorbic acid and 20 mmol/l sodium pyruvate. The slices from the HL and HCCs of each mouse were randomly divided into three groups, one non-irradiated and two for irradiation with different doses, and placed in twelve different plates. All slices were cultured in an incubator under constant conditions of 37° C and 5% CO_2. On the next day, at 05:00 am, the medium was changed and this time point was defined as CT00. 2 hours after the medium change (CT02), the plates were removed from the culturing conditions and transferred to the irradiation lab in a cooler to reduce the possible changes in the ambient temperature. The slices were irradiated at four different CTs (CT02, CT08, CT14 and CT20) with two different doses, 2 Gy (at 175 kV and 15 mA, for about 2 min) and 10 Gy (at 175 kV and 15 mA, for about 10 min), using Gulmay RS225 X-ray system (X-Strahl, Camberley, UK). Non-irradiated slices were

Preprints (www.preprints.org) | NOT PEER-REVIEWED | Posted: 29 January 2021 doi:10.20944/preprints202101.0603.v1

transported to the irradiation lab but did not receive irradiation. Within one hour after irradiation, the slices were returned to regular culturing conditions. 48 hours after irradiation, the slices were harvested at the same CTs used for irradiation. For immunohistochemistry, the slices were fixed in 4% paraformaldehyde (PFA) in phosphate buffered saline (0.1 M PBS, pH 7.4) for 12 hours and then cryoprotected with gradually increasing concentrations of sucrose in PBS (15% and 30%). Then the slices were cut into 10 µm thick serial sections using a cryostat (Leica CM, Wetzlar, Germany).

Irradiation of mice and *ex vivo* analyses

Forty-eight HCC bearing mice (7-10 month old) were used for *ex vivo* investigations and randomly divided into 2 groups: the first group comprised 24 animals which were irradiated with a dose of 10 Gy (irradiated group) at four different ZTs (ZT02, ZT08, ZT14 and ZT20). The second group comprised 24 mice with HCC which were transported to the irradiation lab together with the animals of the irradiated group at the same ZTs but they were not subjected to irradiation (non-irradiated group) to omit the effect of transportation.

For irradiation, the mice were deeply anesthetized by intraperitoneal injection with a mixture of ketamine (100 mg/kg body weight, Inresa, Freiburg, Germany) and xylazine (10 mg/kg body weight, Rompun 2%, Bayer Leverkusen, Germany) and fixed on a styrofoam plate so that their ventral side was exposed to the irradiation source. Exposure with 10 Gy irradiation was performed as described above (OSCs).

48 hours later, the irradiated and non-irradiated mice (n= 6/ZT in each group) were sacrificed at the same ZTs used for irradiation. Blood was collected from the right atrium in EDTA blood tubes and quickly mixed to avoid coagulation. In addition, the blood cells were analyzed in a control group which did not receive any treatment. The complete blood counts (CBC) were measured automatically using Scil Vet abc, animal blood count machine (Scil, Viernheim, Germany).

Each group of mice was randomly divided into two subgroups (n=3/ZT) which were used for either immunohistochemistry or real-time PCR analysis. For immunofluorescence, the animals were anesthetized as mentioned above and then perfused transcardially with NaCl (0.9%) for 1 min followed by approximately 100 ml 4% PFA in PBS for 15 min. Perfusion during the night was performed under dim

Preprints (www.preprints.org) | NOT PEER-REVIEWED | Posted: 29 January 2021 doi:10.20944/preprints202101.0603.v1

red light. HL and HCCs were excised and separated by a scalpel. Then the tissues were post-fixed for 2 hours in 4% PFA in PBS, cryoprotected with gradually increasing concentrations of sucrose in PBS (10%, 20%, and 30%) and cut into 12 µm thick serial frozen sections using a cryostat.

For real-time PCR, the mice were sacrificed and HL and HCCs were freshly dissected, rapidly snap frozen in liquid nitrogen and stored at -80° C until further use. The experimental design is shown in Supplementary Figure S5.

Immunofluorescence

Sections from OSC and *ex vivo* samples were incubated with normal goat serum (1:20) diluted in PBS with 0.3% Triton (PBST) for 1 hour at room temperature (RT) to minimize non-specific staining. Then the sections were incubated with the primary antibodies against Ki67 (1:200, #KI6891C01, DCS, Hamburg, Germany) or against γ-H2AX (1:200, #2577, Cell Signaling Technology, Frankfurt am Main, Germany) overnight at RT. The primary antibodies were diluted in 1% bovine serum albumin (BSA) in PBST. On the next day, sections were incubated with secondary goat anti rabbit antibodies (Alexa Fluor 568 for Ki67 or Alexa Fluor 488 for γ-H2AX) in PBS (1:250, Life Technologies, San Diego, CA, USA) for 1 hour in darkness at RT. For negative control, the primary antibodies were omitted and sections were only incubated with the secondary antibodies. For nuclear staining, all sections were incubated with Hoechst dye diluted in PBS (1:10000) for 10 min in darkness at RT. The sections were then covered with fluorescent mounting media (Fluoromount-G, Southern Biotech, Germany).

Sections were analyzed using Keyence BZ-X800 series microscope (Keyence, Osaka, Japan) using x20 objective and the settings were kept constant for each staining. Six representative images at least from each animal/time point/group were analyzed and averaged. The number of immunoreactive (+) cells was counted by an investigator blind to the treatment. The number of positive cells was counted manually in each image in a total area= 0.4 mm^2.

Real-time PCR

Total RNA from *ex vivo* samples was extracted using RNeasy Plus Universal Mini Kit (QIAGEN, Hilden, Germany). Total RNA concentration and purity were

Preprints (www.preprints.org) | NOT PEER-REVIEWED | Posted: 29 January 2021 doi:10.20944/preprints202101.0603.v1

measured using a Nano-Drop spectrophotometer. Revert Aid First Strand cDNA Synthesis Kit (Thermo Scientific, Vilnius, Lithuania) was used for the synthesis of the cDNA from 1 µg RNA. Primers for the clock genes *Per1*, *Per2*, *Cry1*, *Cry2*, *Clock*, *Bmal1*, and *Rev-erbα* (Sigma Aldrich, Germany, Table 1) and the housekeeping gene, β-actin, were validated using conventional PCR and gel electrophoresis. Real-time PCR was performed using Step One Plus (Applied Biosystems) and SYBR GREEN (Kapa Abi-Prism). The relative mRNA expression of the clock genes, normalized to the housekeeping gene, was calculated according to Pfaffl method [67].

Table (1): List of primer sequences used in qPCR

Gene	Primer sequence
β-Actin F	**5´ –GGCTGTATTCCCCTCCATGC- 3´**
β-Actin R	**5´ –CCAGTTGGTAACAATGCCATGT- 3´**
mPer1 F	**5´ –TGG CTC AAG TGG CAA TGA GTC - 3´**
mPer1 R	**5´ –GGC TCG AGC TGA CTG TTC ACT - 3´**
mPer2 F	**5´ –CCAAACTGCTTGTTCCAGGC- 3´**
mPer2 R	**5´ –ACCGGCCTGTAGGATCTTCT - 3´**
mCry1 F	**5´ – CTT CTG TCT GAT GAC CAT GAT GA- 3´**
mCry1 R	**5´ – CCC AGG CCT TTC TTT CCA A- 3´**
mCry2 F	**5´ – AGG GCT GCC AAG TGC ATC AT- 3´**
mCry2 R	**5´ – AGG AAG GGA CAG ATG CCA ATA G- 3´**
mClock F	**5´ – CAC CGA CAA AGA TCC CTA CTG AT- 3´**
mClock R	**5´ – TGA GAC ATC GCT GGC TGT GT- 3´**
Bmal F	**5´ –GTA GAT CAG AGG GCG ACA GC- 3´**
Bmal R	**5´ –CCT GTG ACA TTC TGC GAG GT- 3´**
Rev-erbα F	**5´ –GGT GCG CTT TGC ATC GTT- 3´**
Rev-erbα R	**5´ –GGT TGT GCG GCT CAG GAA- 3´**

Preprints (www.preprints.org) | NOT PEER-REVIEWED | Posted: 29 January 2021 doi:10.20944/preprints202101.0603.v1

Statistical analysis

Statistics were calculated using Graph Pad Prism 8 software. For *in vitro* experiments, repeated measure analysis of variance (ANOVA) was used. For *ex vivo* experiments, ordinary one-way ANOVA followed by *Tukey's* test for multiple comparisons among different time points was performed. Effect of time and treatment was analyzed by two-way ANOVA followed by *Sidak's* test for multiple comparisons. The results were represented as mean ± standard error of the mean (SEM) and were regarded as significant at $p < 0.05$.

Conclusions

Our study showed time-dependent effects of radiotherapy on proliferation rate, DNA damage/repair, clock gene expression, and white blood cells. The late activity phase (ZT20) might be the most favorable time for application of radiotherapy as the effects on the tumor are high and the side effects on the surrounding HL and on the total leukocyte number are lowest at this time point. Moreover, at this time point irradiation had no effect on clock gene expression in HL. It now needs a translational approach to analyze whether also in humans the late activity phase (ZT08) would be the optimal time point for radiotherapy of HCC. The comparison between *in vitro* (OSC) data and *ex vivo* results from whole animals shows that *in vitro* experiments may be useful to determine the dosage, because the effects of irradiation were dose-dependent. However, with regard to the time course of proliferation, DNA-DSBs and radiosensitivity, there were substantial differences between *in vitro* and *ex vivo* samples. Thus, under the conditions used in our study, OSC is of limited value. While they may help to determine dose-dependent effects, they are not suited to design chronotherapeutic approaches.

Preprints (www.preprints.org) | NOT PEER-REVIEWED | Posted: 29 January 2021 doi:10.20944/preprints202101.0603.v1

Supplementary materials

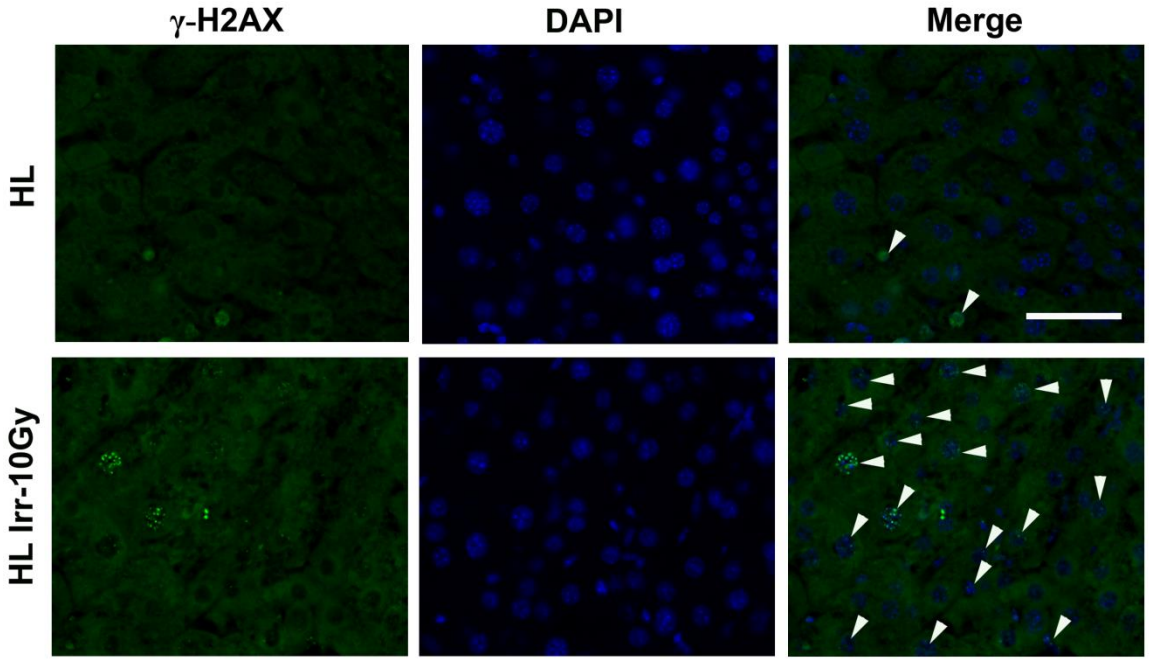

Fig. S1 Representative high magnification photomicrographs of γ-H2AX immunoreactive (+) (green) in DAPI stained nuclei (blue) in healthy liver (HL) without or with irradiation (Irr-10Gy) at ZT02. γ-H2AX + cells were defined by co-localization of γ-H2AX foci (arrows) and DAPI. Scale bar, 50 μm.

Preprints (www.preprints.org) | NOT PEER-REVIEWED | Posted: 29 January 2021 doi:10.20944/preprints202101.0603.v1

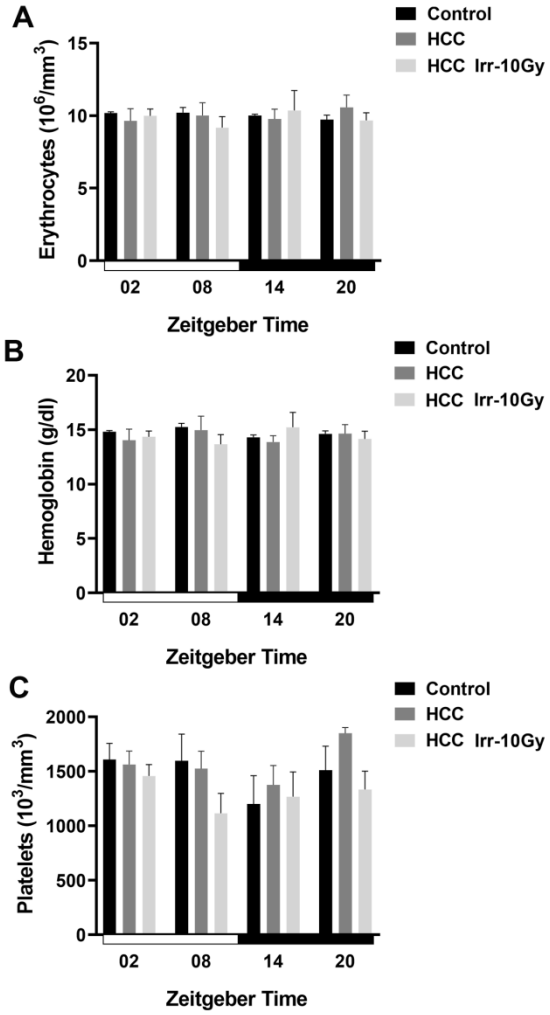

Fig. S2 Blood cell analysis in control and hepatocellular carcinoma (HCC) bearing mice without and with irradiation. At different *Zeitgeber* times (ZT00= the onset of the light phase), mice were irradiated (Irr) with a dose of 10 Gy (n= 3-6/time point) or handled similarly but not irradiated. 48 hours later, mice were sacrificed and the blood was collected at the same ZTs. Erythrocyte numbers (**A**). Hemoglobin concentration (**B**). Platelet numbers (**C**). Plotted are the mean numbers ± SEM. White and black bars indicate the light and dark phases, respectively.

Preprints (www.preprints.org) | NOT PEER-REVIEWED | Posted: 29 January 2021 doi:10.20944/preprints202101.0603.v1

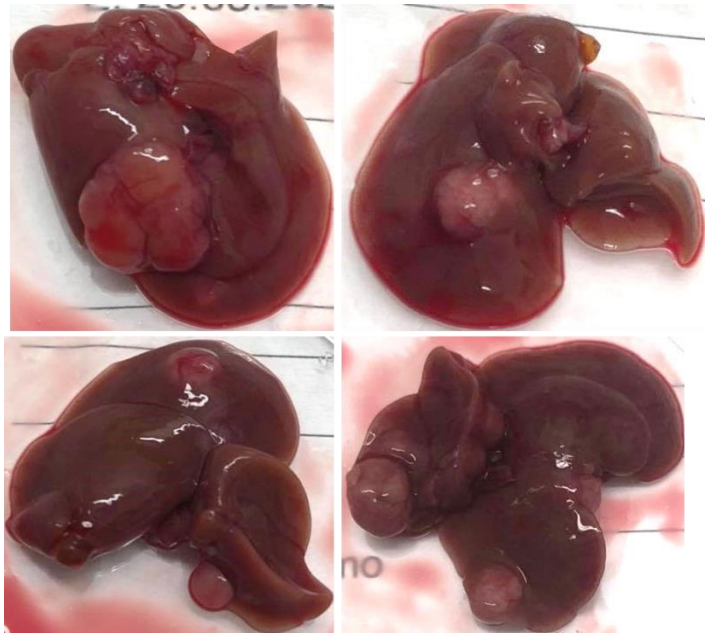

Fig. S3 Representative photographs of single and multiple hepatocellular carcinomas (HCC) at the age of 7-10 months. The mice received a single injection of diethylnitrosamine (DEN) at the age of two weeks and chronic treatment of phenobarbital (PB) in the drinking water to accelerate the HCC induction.

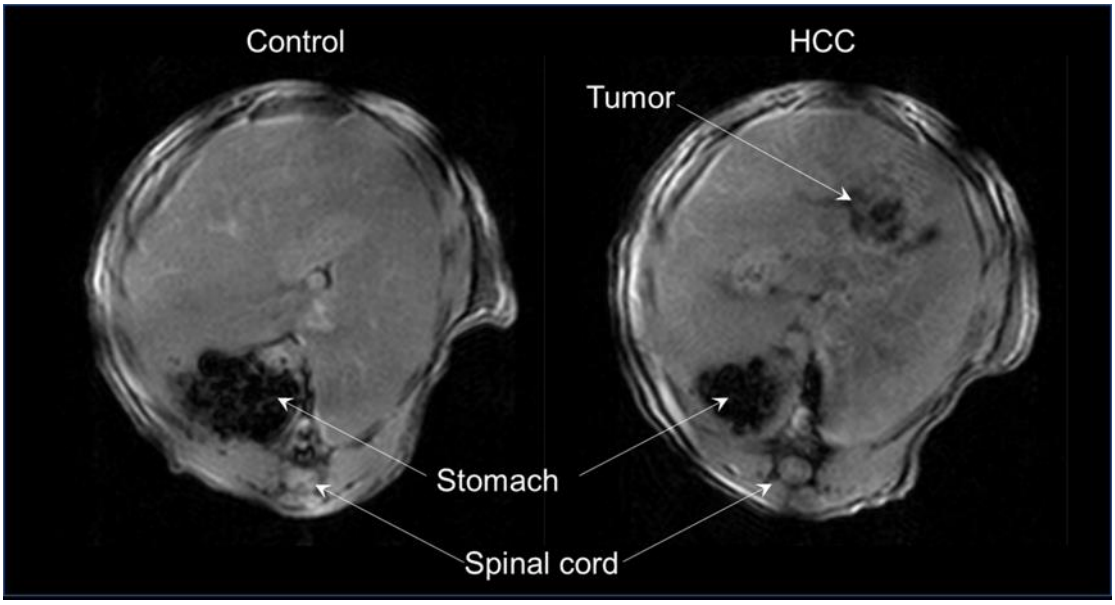

Fig. S4 Representative axial MRI images from healthy and HCC bearing mice demonstrating the unequivocal identification of tumor tissue within the liver.

Preprints (www.preprints.org) | NOT PEER-REVIEWED | Posted: 29 January 2021 doi:10.20944/preprints202101.0603.v1

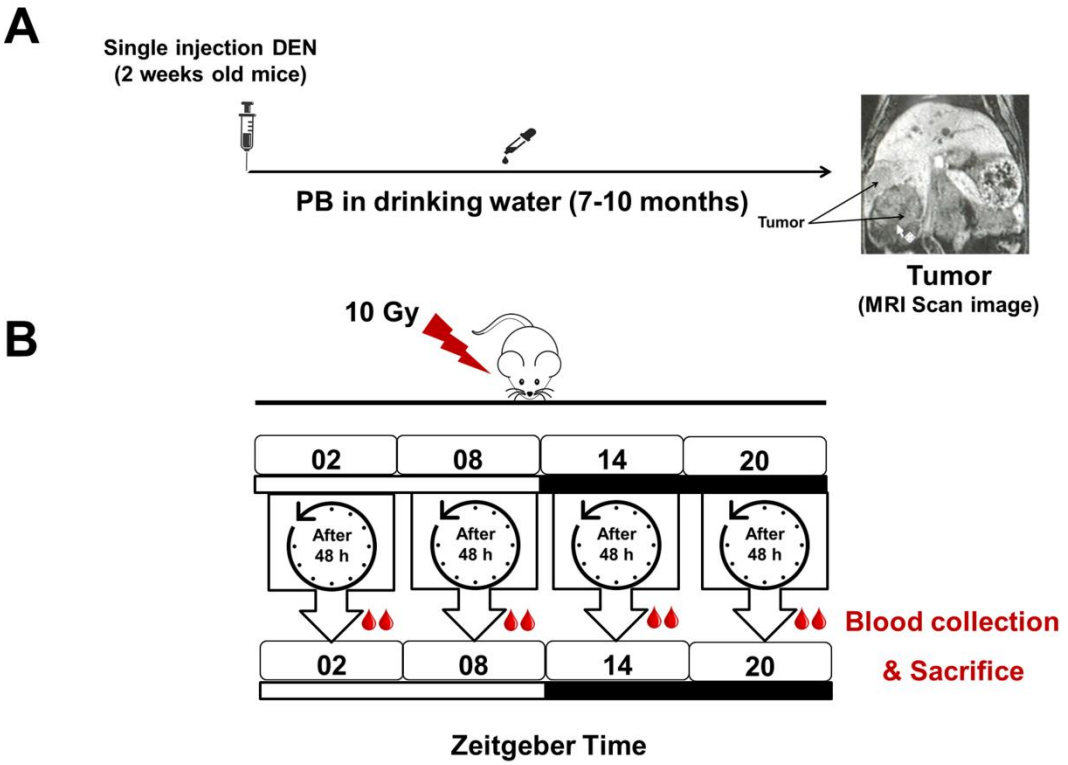

Fig. S3 Diagram for the experimental design of tumor induction, animals' irradiation and *ex vivo* analyses. **A,** Transgenic *Per2::luc* mice (n=48 mice) received a single injection of diethylnitrosamine (DEN) at the age of two weeks and chronic treatment of phenobarbital (PB) in the drinking water to accelerate the hepatocellular carcinoma (HCC) induction. HCC developed in animals in either single or multiple tumors at the age of 7-10 months. Tumor development was screened via magnetic resonance imaging (MRI) and validated by post mortem inspection. **B,** 24 animals of the HCC bearing mice were selected for irradiation with a dose of 10 Gy at four different *Zeitgeber* time (ZT) points (ZT02, ZT08, ZT14 and ZT20) (6 animals per time point). 48 hours later, blood was collected and animals were sacrificed at the same ZTs used for irradiation. 12 animals (n=3/ZT) were perfused for immunohistochemistry and 12 animals (n=3/ZT) were used for real-time PCR by collecting and snap freezing the native tissue. White and black bars indicate the light and dark phases, respectively.

Funding

S. A. H. is supported by German Egyptian Research Long-term Scholarship (GERLS) Program of the DAAD. We acknowledge support by the Heinrich-Heine-University Düsseldorf for open access funding.

Acknowledgements

We thank Dr. Julia Hesse (Department of Molecular Cardiology, Heinrich-Heine-University, Düsseldorf, Germany) for facilitating the *in vitro* experiments in her department. We thank Ursula Lammersen, Angelika Hallenberger, Hanna Bellert and Ralf Fassbender for excellent technical support.

Author contributions

Soha A. Hassan: concept/design, acquisition, analysis and interpretation of data and drafting of the manuscript. **Amira A. H. Ali:** acquisition of data and organization of figures. **Dennis Sohn:** acquisition of data. **Ulrich Flögel:** acquisition of data. **Reiner U. Jänicke:** critical revision of the manuscript. **Horst-Werner Korf:** concept/design, acquisition and interpretation of data, supervision and drafting of the manuscript. **Charlotte von Gall:** data interpretation and drafting of the manuscript. All authors have read and approved the manuscript.

Institutional review board statement

Animals were used according to accepted standards of humane animal care and federal guidelines and Directive 2010/63/EU of the European Union. All experiments were approved by the Regierungspräsidium Darmstadt and the Landesamt für Natur, Umwelt und Verbraucherschutz NRW (Reference number: AZ 81-02.04.2018-A146).

Conflict of interest

The authors have no conflict of interest.

References

1. Globocan. Liver cancer fact sheet **2019**.
2. IARC. Latest global cancer data: Cancer burden rises to 18.1 million new cases and 9.6 million cancer deaths in 2018. *PRESS RELEASE* **2018**, *N° 263*
3. Sanchez, D.I.; Gonzalez-Fernandez, B.; Crespo, I.; San-Miguel, B.; Alvarez, M.; Gonzalez-Gallego, J.; Tunon, M.J. Melatonin modulates dysregulated circadian clocks in mice with diethylnitrosamine-induced hepatocellular carcinoma. *Journal of Pineal Research* **2018**, *65*, doi:ARTN e1250610.1111/jpi.12506.
4. Wild, A.T.; Gandhi, N.; Chettiar, S.T.; Aziz, K.; Gajula, R.P.; Williams, R.D.; Kumar, R.; Taparra, K.; Zeng, J.; Cades, J.A., et al. Concurrent versus sequential sorafenib therapy in combination with radiation for hepatocellular carcinoma. *Plos One* **2013**, *8*, e65726, doi:10.1371/journal.pone.0065726.
5. Rebouissou, S.; La Bella, T.; Rekik, S.; Imbeaud, S.; Calatayud, A.L.; Rohr-Udilova, N.; Martin, Y.; Couchy, G.; Bioulac-Sage, P.; Grasl-Kraupp, B., et al. Proliferation Markers Are Associated with MET Expression in Hepatocellular Carcinoma and Predict Tivantinib Sensitivity In Vitro. *Clin Cancer Res* **2017**, *23*, 4364-4375, doi:10.1158/1078-0432.CCR-16-3118.
6. Eriguchi, M.; Levi, F.; Hisa, T.; Yanagie, H.; Nonaka, Y.; Takeda, Y. Chronotherapy for cancer. *Biomedicine & Pharmacotherapy* **2003**, *57*, 92-95, doi:10.1016/j.biopha.2003.08.012.
7. Innominato, P.F.; Levi, F.A.; Bjarnason, G.A. Chronotherapy and the molecular clock: Clinical implications in oncology. *Adv Drug Deliv Rev* **2010**, *62*, 979-1001, doi:10.1016/j.addr.2010.06.002.
8. Mandal, A.S.; Biswas, N.; Karim, K.M.; Guha, A.; Chatterjee, S.; Behera, M.; Kuotsu, K. Drug delivery system based on chronobiology--A review. *J Control Release* **2010**, *147*, 314-325, doi:10.1016/j.jconrel.2010.07.122.
9. Li, H.X. The role of circadian clock genes in tumors. *Onco Targets Ther* **2019**, *12*, 3645-3660, doi:10.2147/OTT.S203144.
10. Ohri, N.; Dawson, L.A.; Krishnan, S.; Seong, J.; Cheng, J.C.; Sarin, S.K.; Kinkhabwala, M.; Ahmed, M.M.; Vikram, B.; Coleman, C.N., et al. Radiotherapy for Hepatocellular Carcinoma: New Indications and Directions for Future Study. *J Natl Cancer Inst* **2016**, *108*, doi:10.1093/jnci/djw133.
11. Chen, C.P. Role of Radiotherapy in the Treatment of Hepatocellular Carcinoma. *J Clin Transl Hepatol* **2019**, *7*, 183-190, doi:10.14218/JCTH.2018.00060.
12. Hassan, S.A.; Schmithals, C.; von Harten, M.; Piiper, A.; Korf, H.-W.; von Gall, C. Time-dependent changes in proliferation, DNA damage and clock gene expression in hepatocellular carcinoma and healthy liver of a transgenic mouse model. *International Journal of Cancer* **2021**, *148*, 226-237, doi:https://doi.org/10.1002/ijc.33228.
13. Harper, E.; Talbot, C.J. Is it Time to Change Radiotherapy: The Dawning of Chronoradiotherapy? *Clin Oncol (R Coll Radiol)* **2019**, *31*, 326-335, doi:10.1016/j.clon.2019.02.010.
14. Muller, M.H.; Rodel, F.; Rub, U.; Korf, H.W. Irradiation with X-rays phase-advances the molecular clockwork in liver, adrenal gland and pancreas. *Chronobiol Int* **2015**, *32*, 27-36, doi:10.3109/07420528.2014.949735.
15. Shih, H.C.; Shiozawa, T.; Kato, K.; Imai, T.; Miyamoto, T.; Uchikawa, J.; Nikaido, T.; Konishi, I. Immunohistochemical expression of cyclins, cyclin-dependent kinases, tumor-suppressor gene products, Ki-67, and sex steroid receptors in endometrial

carcinoma: positive staining for cyclin A as a poor prognostic indicator. *Hum Pathol* **2003**, *34*, 471-478.

16. Johnson, K.; Chang-Claude, J.; Critchley, A.M.; Kyriacou, C.; Lavers, S.; Rattay, T.; Seibold, P.; Webb, A.; West, C.; Symonds, R.P., et al. Genetic Variants Predict Optimal Timing of Radiotherapy to Reduce Side-effects in Breast Cancer Patients. *Clin Oncol (R Coll Radiol)* **2019**, *31*, 9-16, doi:10.1016/j.clon.2018.10.001.
17. Shukla, P.; Gupta, D.; Bisht, S.S.; Pant, M.C.; Bhatt, M.L.; Gupta, R.; Srivastava, K.; Gupta, S.; Dhawan, A.; Mishra, D., et al. Circadian variation in radiation-induced intestinal mucositis in patients with cervical carcinoma. *Cancer* **2010**, *116*, 2031-2035, doi:10.1002/cncr.24867.
18. Rahn, D.A., 3rd; Ray, D.K.; Schlesinger, D.J.; Steiner, L.; Sheehan, J.P.; O'Quigley, J.M.; Rich, T. Gamma knife radiosurgery for brain metastasis of nonsmall cell lung cancer: is there a difference in outcome between morning and afternoon treatment? *Cancer* **2011**, *117*, 414-420, doi:10.1002/cncr.25423.
19. Kuo, L.J.; Yang, L. γ-H2AX – A Novel Biomarker for DNA Double-strand Breaks. *in vivo* **2008**, *22*, 305-310.
20. Sedelnikova, O.A.; Bonner, W.M. GammaH2AX in cancer cells: a potential biomarker for cancer diagnostics, prediction and recurrence. *Cell Cycle* **2006**, *5*, 2909-2913, doi:10.4161/cc.5.24.3569.
21. Liu, C.Y.; Hsieh, C.H.; Kim, S.H.; Wang, J.P.; Ni, Y.L.; Su, C.L.; Yao, C.F.; Fang, K. An indolylquinoline derivative activates DNA damage response and apoptosis in human hepatocellular carcinoma cells. *Int J Oncol* **2016**, *49*, 2431-2441, doi:10.3892/ijo.2016.3717.
22. Liu, S.L.; Han, Y.; Zhang, Y.; Xie, C.Y.; Wang, E.H.; Miao, Y.; Li, H.Y.; Xu, H.T.; Dai, S.D. Expression of metastasis-associated protein 2 (MTA2) might predict proliferation in non-small cell lung cancer. *Target Oncol* **2012**, *7*, 135-143, doi:10.1007/s11523-012-0215-z.
23. Ye, H.; Yang, K.; Tan, X.M.; Fu, X.J.; Li, H.X. Daily rhythm variations of the clock gene PER1 and cancer-related genes during various stages of carcinogenesis in a golden hamster model of buccal mucosa carcinoma. *Oncotargets and Therapy* **2015**, *8*, doi:10.2147/Ott.S83710.
24. Wood, P.A.; Du-Quiton, J.; You, S.; Hrushesky, W.J. Circadian clock coordinates cancer cell cycle progression, thymidylate synthase, and 5-fluorouracil therapeutic index. *Mol Cancer Ther* **2006**, *5*, 2023-2033, doi:10.1158/1535-7163.MCT-06-0177.
25. Zhou, D.; Wang, Y.; Chen, L.; Jia, L.; Yuan, J.; Sun, M.; Zhang, W.; Wang, P.; Zuo, J.; Xu, Z., et al. Evolving roles of circadian rhythms in liver homeostasis and pathology. *Oncotarget* **2016**, *7*, 8625-8639, doi:10.18632/oncotarget.7065.
26. Schibler, U.; Ripperger, J.; Brown, S.A. Peripheral circadian oscillators in mammals: time and food. *J Biol Rhythms* **2003**, *18*, 250-260, doi:10.1177/0748730403018003007.
27. Korf, H.-W.; von Gall, C. Circadian Physiology. In *Neuroscience in the 21st Century: From Basic to Clinical*, Pfaff, D.W., Ed. Springer New York: New York, NY, 2013; 10.1007/978-1-4614-1997-6_65pp. 1813-1845.
28. Huisman, S.A.; Oklejewicz, M.; Ahmadi, A.R.; Tamanini, F.; Ijzermans, J.N.; van der Horst, G.T.; de Bruin, R.W. Colorectal liver metastases with a disrupted circadian rhythm phase shift the peripheral clock in liver and kidney. *Int J Cancer* **2015**, *136*, 1024-1032, doi:10.1002/ijc.29089.
29. Yang, F.E.; Vaida, F.; Ignacio, L.; Houghton, A.; Nauityal, J.; Halpern, H.; Sutton, H.; Vijayakumar, S. Analysis of weekly complete blood counts in patients receiving standard fractionated partial body radiation therapy. *Int J Radiat Oncol Biol Phys* **1995**, *33*, 617-617.

30. Wersal, C.; Keller, A.; Weiss, C.; Giordano, F.; Abo-Madyan, Y.; Tuschy, B.; Suetterlin, M.; Wenz, F.; Sperk, E. Long-term changes in blood counts after intraoperative radiotherapy for breast cancer—single center experience and review of the literature. *Translational Cancer Research* **2019**, *8*, 1882-1903, doi:10.21037/tcr.2019.09.05.
31. Vucic, V.; Isenovic, E.R.; Adzic, M.; Ruzdijic, S.; Radojcic, M.B. Effects of gamma-radiation on cell growth, cycle arrest, death, and superoxide dismutase expression by DU 145 human prostate cancer cells. *Braz J Med Biol Res* **2006**, *39*, 227-236, doi:10.1590/s0100-879x2006000200009.
32. Schwarz-Finsterle, J.; Scherthan, H.; Huna, A.; González, P.; Mueller, P.; Schmitt, E.; Erenpreisa, J.; Hausmann, M. Volume increase and spatial shifts of chromosome territories in nuclei of radiation-induced polyploidizing tumour cells. *Mutation Research/Genetic Toxicology and Environmental Mutagenesis* **2013**, *756*, 56-65, doi:https://doi.org/10.1016/j.mrgentox.2013.05.004.
33. You, S.; Wood, P.A.; Xiong, Y.; Kobayashi, M.; Du-Quiton, J.; Hrushesky, W.J. Daily coordination of cancer growth and circadian clock gene expression. *Breast Cancer Res Treat* **2005**, *91*, 47-60, doi:10.1007/s10549-004-6603-z.
34. Echave Llanos, J.M.; Nash, R.E. Mitotic circadian rhythm in a fast-growing and a slow-growing hepatoma: mitotic rhythm in hepatomas. *J Natl Cancer Inst* **1970**, *44*, 581-585.
35. Klevecz, R.R.; Braly, P.S. Circadian and ultradian rhythms of proliferation in human ovarian cancer. *Chronobiol Int* **1987**, *4*, 513-523.
36. Fu, L.; Pelicano, H.; Liu, J.; Huang, P.; Lee, C. The circadian gene Period2 plays an important role in tumor suppression and DNA damage response in vivo. *Cell* **2002**, *111*, 41-50, doi:10.1016/s0092-8674(02)00961-3.
37. Yang, X.; Wood, P.A.; Ansell, C.M.; Quiton, D.F.; Oh, E.Y.; Du-Quiton, J.; Hrushesky, W.J. The circadian clock gene Per1 suppresses cancer cell proliferation and tumor growth at specific times of day. *Chronobiol Int* **2009**, *26*, 1323-1339, doi:10.3109/07420520903431301.
38. Wang, J.S.; Wang, H.J.; Qian, H.L. Biological effects of radiation on cancer cells. *Mil Med Res* **2018**, *5*, 20, doi:10.1186/s40779-018-0167-4.
39. Buhr, E.D.; Yoo, S.H.; Takahashi, J.S. Temperature as a universal resetting cue for mammalian circadian oscillators. *Science* **2010**, *330*, 379-385, doi:10.1126/science.1195262.
40. Bur, I.M.; Zouaoui, S.; Fontanaud, P.; Coutry, N.; Molino, F.; Martin, A.O.; Mollard, P.; Bonnefont, X. The comparison between circadian oscillators in mouse liver and pituitary gland reveals different integration of feeding and light schedules. *PLoS One* **2010**, *5*, e15316, doi:10.1371/journal.pone.0015316.
41. Mohawk, J.A.; Green, C.B.; Takahashi, J.S. Central and peripheral circadian clocks in mammals. *Annu Rev Neurosci* **2012**, *35*, 445-462, doi:10.1146/annurev-neuro-060909-153128.
42. Matsuo, T.; Yamaguchi, S.; Mitsui, S.; Emi, A.; Shimoda, F.; Okamura, H. Control mechanism of the circadian clock for timing of cell division in vivo. *Science* **2003**, *302*, 255-259, doi:10.1126/science.1086271.
43. Huisman, S.A.; Ahmadi, A.R.; JN, I.J.; Verhoef, C.; van der Horst, G.T.; de Bruin, R.W. Disruption of clock gene expression in human colorectal liver metastases. *Tumour Biol* **2016**, *37*, 13973-13981, doi:10.1007/s13277-016-5231-7.
44. Mteyrek, A.; Filipski, E.; Guettier, C.; Okyar, A.; Levi, F. Clock gene Per2 as a controller of liver carcinogenesis. *Oncotarget* **2016**, *7*, 85832-85847, doi:10.18632/oncotarget.11037.

45. Deng, F.; Yang, K. Current Status of Research on the Period Family of Clock Genes in the Occurrence and Development of Cancer. *J Cancer* **2019**, *10*, 1117-1123, doi:10.7150/jca.29212.
46. Oshima, T.; Takenoshita, S.; Akaike, M.; Kunisaki, C.; Fujii, S.; Nozaki, A.; Numata, K.; Shiozawa, M.; Rino, Y.; Tanaka, K., et al. Expression of circadian genes correlates with liver metastasis and outcomes in colorectal cancer. *Oncol Rep* **2011**, *25*, 1439-1446, doi:10.3892/or.2011.1207.
47. Lin, Y.M.; Chang, J.H.; Yeh, K.T.; Yang, M.Y.; Li, T.C.; Lin, S.F.; Su, W.W.; Chang, J.G. Disturbance of Circadian Gene Expression in Hepatocellular Carcinoma. *Molecular Carcinogenesis* **2008**, *47*, 925-933, doi:10.1002/mc.20446.
48. Sotak, M.; Polidarova, L.; Ergang, P.; Sumova, A.; Pacha, J. An association between clock genes and clock-controlled cell cycle genes in murine colorectal tumors. *International Journal of Cancer* **2013**, *132*, 1032-1041, doi:10.1002/ijc.27760.
49. Morgan, M.; Dvuchbabny, S.; Martinez, C.-A.; Kerr, B.; Cistulli, P.A.; Cook, K.M. The Cancer Clock Is (Not) Ticking: Links between Circadian Rhythms and Cancer. *Clocks & Sleep* **2019**, *1* 435–458, doi:doi:10.3390/clockssleep1040034.
50. Hunyor, I.; Cook, K.M. Models of intermittent hypoxia and obstructive sleep apnea: molecular pathways and their contribution to cancer. *Am J Physiol-Reg I* **2018**, *315*, R669-R687, doi:10.1152/ajpregu.00036.2018.
51. Yu, C.; Yang, S.L.; Fang, X.; Jiang, J.X.; Sun, C.Y.; Huang, T. Hypoxia disrupts the expression levels of circadian rhythm genes in hepatocellular carcinoma. *Mol Med Rep* **2015**, *11*, 4002-4008, doi:10.3892/mmr.2015.3199.
52. Mormont, M.C.; Levi, F. Cancer chronotherapy: Principles, applications, and perspectives. *Cancer* **2003**, *97*, 155-169, doi:10.1002/cncr.11040.
53. Lu, H.; Chu, Q.; Xie, G.; Han, H.; Chen, Z.; Xu, B.; Yue, Z. Circadian gene expression predicts patient response to neoadjuvant chemoradiation therapy for rectal cancer. *Int J Clin Exp Pathol* **2015**, *8*, 10985-10994.
54. Shuboni-Mulligan, D.D.; Breton, G.; Smart, D.; Gilbert, M.; Armstrong, T.S. Radiation chronotherapy-clinical impact of treatment time-of-day: a systematic review. *J Neurooncol* **2019**, *145*, 415-427, doi:10.1007/s11060-019-03332-7.
55. Antoch, M.P.; Kondratov, R.V.; Takahashi, J.S. Circadian clock genes as modulators of sensitivity to genotoxic stress. *Cell Cycle* **2005**, *4*, 901-907, doi:10.4161/cc.4.7.1792.
56. Dakup, P.P.; Porter, K.I.; Gajula, R.P.; Goel, P.N.; Cheng, Z.; Gaddameedhi, S. The circadian clock protects against ionizing radiation-induced cardiotoxicity. *Faseb J* **2020**, *34*, 3347-3358, doi:10.1096/fj.201901850RR.
57. Ohkura, N.; Oishi, K.; Sekine, Y.; Atsumi, G.-i.; Ishida, N.; Matsuda, J.; Horie, S. Comparative Study of Circadian Variation in Numbers of Peripheral Blood Cells among Mouse Strains: Unique Feature of C3H/HeN Mice. *Biological and Pharmaceutical Bulletin* **2007**, *30*, 1177-1180, doi:10.1248/bpb.30.1177.
58. Hassan, S.A.; Ali, A.A.H.; Yassine, M.; Sohn, D.; Pfeffer, M.; Jänicke, R.U.; Korf, H.-W.; von Gall, C. Relationship between locomotor activity rhythm and corticosterone levels during HCC development, progression and treatment in a mouse model. *J. Pineal Res. under review*
59. Nakagawa, M.; Terashima, T.; D'Yachkova, Y.; Bondy, G.P.; Hogg, J.C.; van Eeden, S.F. Glucocorticoid-induced granulocytosis: contribution of marrow release and demargination of intravascular granulocytes. *Circulation* **1998**, *98*, 2307-2313, doi:10.1161/01.cir.98.21.2307.
60. Stone, H.B.; Coleman, C.N.; Anscher, M.S.; McBride, W.H. Effects of radiation on normal tissue: consequences and mechanisms. *Lancet Oncol* **2003**, *4*, 529-536, doi:10.1016/s1470-2045(03)01191-4.

61. Terrones, C.; Specht, L.; Maraldo, M.V.; Lundgren, J.; Helleberg, M. Lymphopenia after Radiotherapy and Risk of Infection. *Open Forum Infectious Diseases* **2017**, *4*, S702-S702, doi:10.1093/ofid/ofx163.1882.
62. Moreno-Smith, M.; Lutgendorf, S.K.; Sood, A.K. Impact of stress on cancer metastasis. *Future oncology (London, England)* **2010**, *6*, 1863-1881, doi:10.2217/fon.10.142.
63. Distelhorst, C.W. Recent insights into the mechanism of glucocorticosteroid-induced apoptosis. *Cell Death & Differentiation* **2002**, *9*, 6-19, doi:10.1038/sj.cdd.4400969.
64. Bray, F.N.; Simmons, B.J.; Wolfson, A.H.; Nouri, K. Acute and Chronic Cutaneous Reactions to Ionizing Radiation Therapy. *Dermatol Ther (Heidelb)* **2016**, *6*, 185-206, doi:10.1007/s13555-016-0120-y.
65. Uribe-Querol, E.; Rosales, C. Neutrophils in Cancer: Two Sides of the Same Coin. *Journal of Immunology Research* **2015**, *2015*, 983698, doi:10.1155/2015/983698.
66. Verrill, C.; Davies, J.; Millward-Sadler, H.; Sundstrom, L.; Sheron, N. Organotypic liver culture in a fluid-air interface using slices of neonatal rat and adult human tissue--a model of fibrosis in vitro. *J Pharmacol Toxicol Methods* **2002**, *48*, 103-110, doi:10.1016/S1056-8719(03)00042-X.
67. Pfaffl, M.W. Quantification strategies in real-time PCR. In: Bustin SA, e.A.-Z.o.q.P., Ed. La Jolla: International University Line (IUL): 2004; pp. 87-112.